ACS NANO

www.acsnano.org

ARTICLE

N-Cadherin Targeted Melanin Nanoparticles Reverse the Endothelial–Mesenchymal Transition in Vascular Endothelial Cells to Potentially Slow the Progression of Atherosclerosis and Cancer

Jinyuan Liu, Xiao Yu, Annaliese Braucht, Steve Smith, and Congzhou Wang*

Cite This: *ACS Nano* 2024, 18, 8229–8247

Read Online

ACCESS | Metrics & More | Article Recommendations | Supporting Information

ABSTRACT: **Endothelial–mesenchymal transition (EndoMT) of vascular endothelial cells has recently been considered as a key player in the early progression of a variety of vascular and nonvascular diseases, including atherosclerosis, cancer, and organ fibrosis. However, current strategies attempting to identify pharmacological inhibitors to block the regulatory pathways of EndoMT suffer from poor selectivity, unwanted side effects, and a heterogeneous response from endothelial cells with different origins. Furthermore, EndoMT inhibitors focus on preventing EndoMT, leaving the endothelial cells that have already undergone EndoMT unresolved. Here, we report the design of a simple but powerful nanoparticle system (i.e., N-cadherin targeted melanin nanoparticles) to convert cytokine-activated, mesenchymal-like endothelial cells back to their original endothelial phenotype. We term this process "Reversed EndoMT" (R-EndoMT). R-EndoMT allows the impaired endothelial barriers to recover their quiescence and intactness, with significantly reduced leukocyte and cancer cell adhesion and transmigration, which could potentially stop atheromatous plaque formation and cancer metastasis in the early stages. R-EndoMT is achieved on different endothelial cell types originating from arteries, veins, and capillaries, independent of activating cytokines. We reveal that N-cadherin targeted melanin nanoparticles reverse EndoMT by downregulating an N-cadherin dependent RhoA activation pathway. Overall, this approach offers a different prospect to treat multiple EndoMT-associated diseases by designing nanoparticles to reverse the phenotypical transition of endothelial cells.**

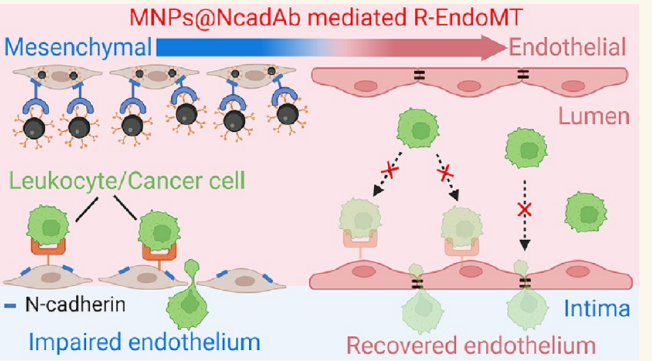

KEYWORDS: *Reversed endothelial–mesenchymal transition (R-EndoMT), N-cadherin, Melanin nanoparticles, Atherosclerosis, Cancer metastasis*

INTRODUCTION

Endothelial–mesenchymal transition (EndoMT) is a newly recognized cell trans-differentiation program in which endothelial cells lose their original phenotype and acquire a mesenchymal phenotype.[1] It is a special form of epithelial–mesenchymal transition (EMT) that hinges on the phenotypical plasticity of endothelial cells.[2] In this process, endothelial cells undergo both morphological and molecular changes, including transformation from cuboidal to spindle shape, loosened cell–cell junctions, reduced expression of endothelial markers (e.g., vascular endothelial cadherin and platelet endothelial cell adhesion molecule-1), and upregulation of mesenchymal markers (e.g., N-cadherin, α-smooth muscle actin, and vimentin).[3] Along with these changes, endothelial-derived mesenchymal cells acquire enhanced cell mobility, invasiveness, and contractility, all of which are typical features of mesenchymal, fibroblast-like cells.[4] EndoMT was initially

Received: December 6, 2023
Revised: February 16, 2024
Accepted: February 23, 2024
Published: March 1, 2024

https://doi.org/10.1021/acsnano.3c12281
ACS Nano 2024, 18, 8229–8247

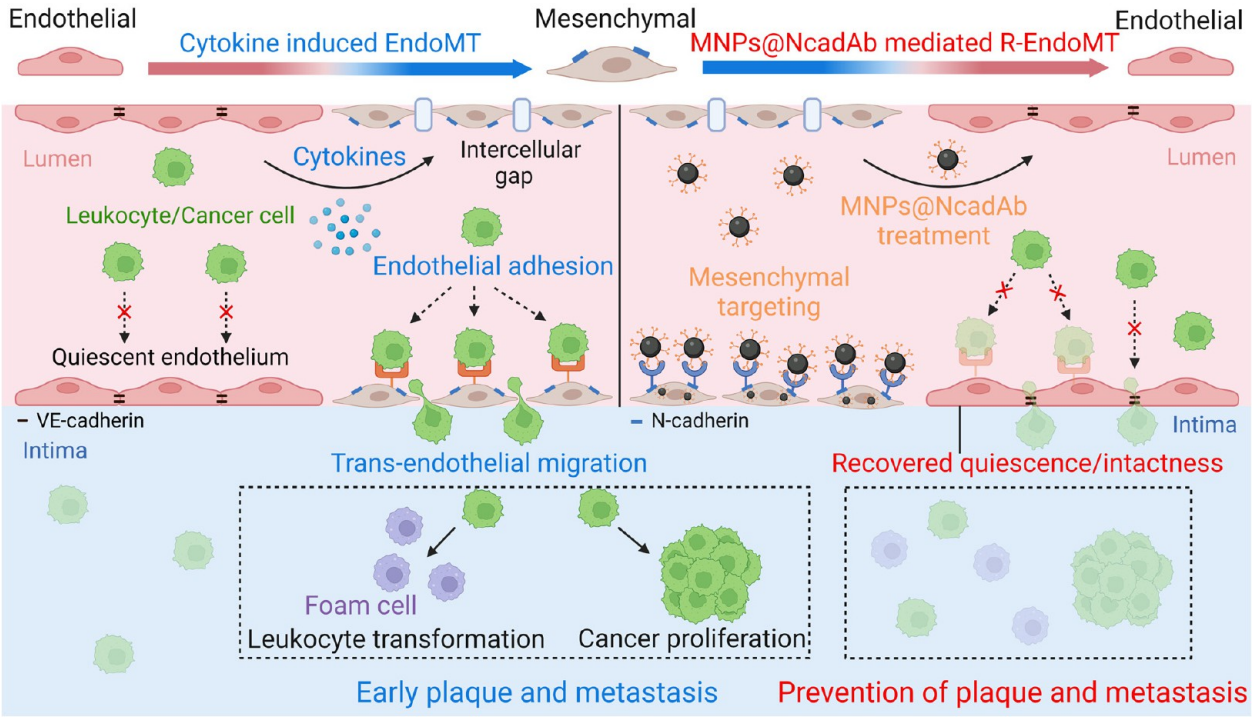

Figure 1. Schematic illustration of "Reversed EndoMT" (R-EndoMT) in endothelial cells mediated by nanoparticles. N-cadherin targeted melanin nanoparticles are designed to target and modulate the endothelial cell plasticity via driving the reversal of cytokine induced EndoMT. We term this process "Reversed EndoMT" (R-EndoMT), switching the mesenchymal phenotype back to the endothelial phenotype. Such phenotypical changes in endothelial cells lead to recovered quiescence and intactness of endothelial barriers, with significantly reduced leukocyte and cancer cell adhesion and transmigration, which could potentially stop or slow atheromatous plaque formation and cancer metastasis in early stages.

discovered as a fundamental mechanism for embryonic development when forming a mesenchymal heart cushion. Recently, a substantial body of evidence has demonstrated that EndoMT can be reactivated postnatally under certain pathological conditions in adulthood, leading to the initiation and progression of multiple vascular and nonvascular diseases such as atherosclerosis and cancer.[5,6] Importantly, a strong correlation has been established between the extent of EndoMT and the severity of these diseases, underscoring the clinical relevance of the EndoMT process.[6−8]

During the onset of atherosclerosis, quiescent endothelial cells can be activated by several biochemical and biomechanical stimuli, such as inflammation or abnormal shear stress, to undergo the EndoMT process.[5,9] The activated endothelial cells then become motile with enhanced paracellular permeability, facilitating the recruitment, infiltration, and accumulation of the endothelial cell-derived mesenchymal cells, blood lipids, and inflammation-related immune cells to the intima of the artery, the hallmarks of early atheromatous plaque formation.[10,11] The plaque-associated mesenchymal cells can produce extracellular matrix and metalloproteases, facilitating plaque build-up and instability, further advancing the progression of atherosclerosis.[12] Interestingly, mounting evidence indicates that EndoMT plays a similar role in cancer progression: During metastasis, cancer cells from primary tumors secrete cytokines and growth factors into blood circulation to trigger the EndoMT of endothelial cells at the remote site of extravasation (mainly in the small capillaries) prior to the arrival of metastatic cancer cells.[13] This "preconditioning" of distant microvasculature leads to increased endothelial permeability, thus opening intercellular gaps for circulating cancer cells to transmigrate into surrounding tissues, a critical step to establish micrometastasis and secondary tumors.[14] Recently, endothelial-derived mesenchymal cells have also been determined to be an important source for cancer-associated fibroblasts, shaping the tumor microenvironment and facilitating tumor progression.[15,16] Based on these aspects of EndoMT, it has been increasingly appreciated that targeting EndoMT holds enormous therapeutic potential and provides a promising approach for treating these diseases.

Currently, the majority of efforts targeting EndoMT focus on identification of pharmacological inhibitors to block the regulatory pathways of EndoMT, especially inhibiting cytokine mediated pathways that cause EndoMT. As the best-studied EndoMT inducer, the canonical cytokine, transforming growth factor beta (TGF-β) signaling, has been a main target to inhibit owing to its tight link to the development of atherosclerosis and metastatic cancer.[8,17,18] However, therapeutic inhibition of TGF-β signaling has been unsuccessful in clinical trials owing to numerous side effects and complications since this family of proteins exert pleiotropic effects on a broad spectrum of crucial cellular functions and regulatory pathways.[3,19,20] Another reason for the failed clinical trials lies in the heterogeneous response to the EndoMT inhibitors from different organotypic endothelial cells originating from arteries, veins, and capillaries.[21] Apart from TGF-β signaling, it is well documented that sustained exposure to pro-inflammatory cytokines such as interleukin-1 beta (IL-1β), tumor necrosis factor alpha (TNF-α), and interferon gamma (IFN-γ) can induce EndoMT in endothelial cells, thus contributing to the development of atherosclerosis, which is generally considered

https://doi.org/10.1021/acsnano.3c12281
ACS Nano 2024, 18, 8229−8247

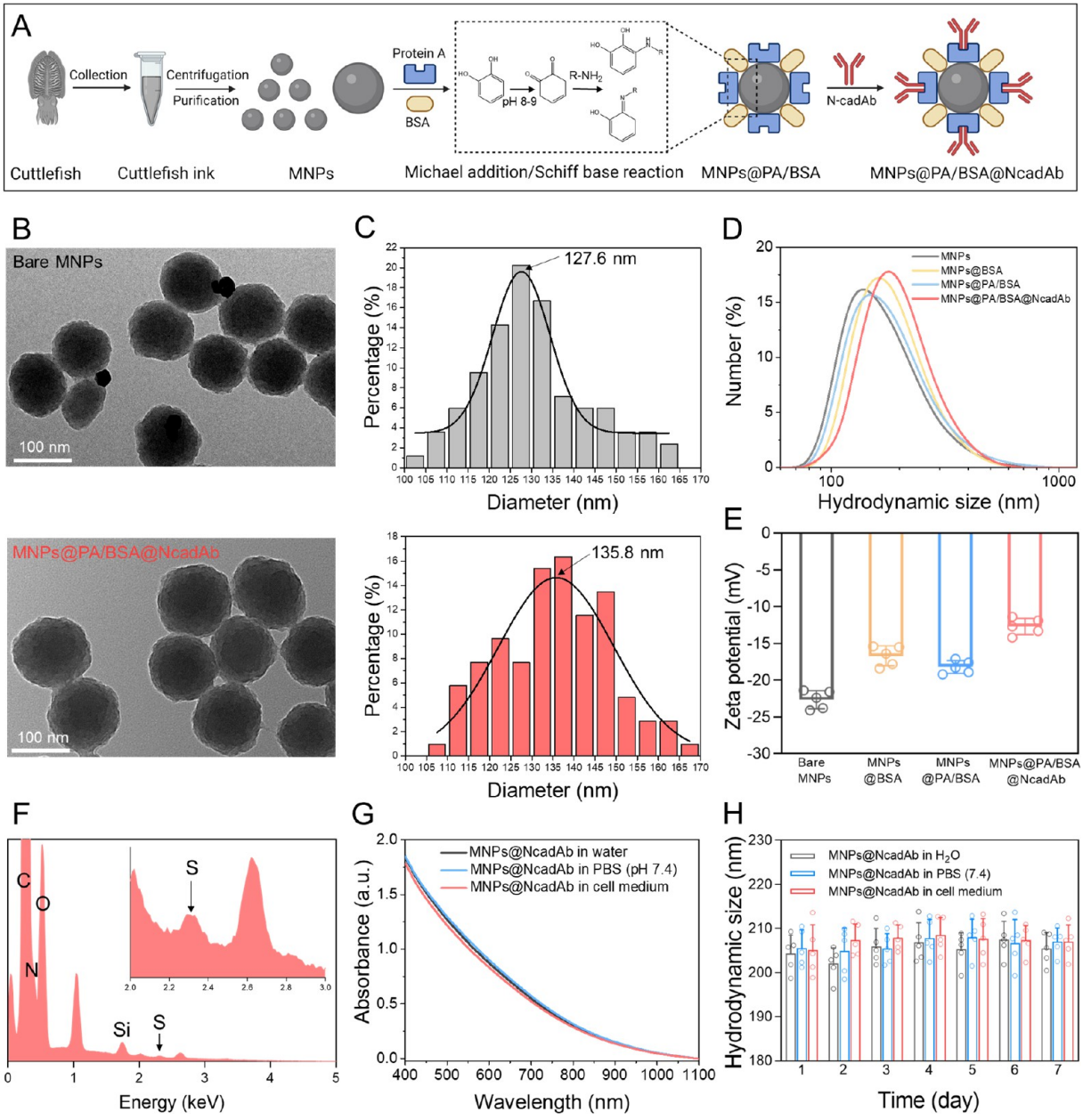

Figure 2. Functionalization and characterization of melanin nanoparticles (MNPs). (A) Schematic illustration of the extraction of natural MNPs from cuttlefish ink and surface functionalization of MNPs with N-cadherin antibody. (B) Transmission electron microscope images of bare and N-cadherin antibody functionalized MNPs. (C) Statistical analysis of nanoparticle size distribution based on the transmission electron microscope images. (D) Hydrodynamic size and (E) zeta potential of bare MNPs, MNP@BSA, MNP@PA/BSA, and MNP@PA/BSA@NcadAb in H_2O. (F) SEM-EDX spectrum of MNP@PA/BSA@NcadAb showing the presence of sulfur because of the disulfide bonds in immunoglobulins. (G) UV−vis absorbance spectrum of MNP@PA/BSA@NcadAb (40 μg/mL) when dispersed in H_2O, PBS buffer, and serum-containing cell culture medium. (H) Hydrodynamic size of MNP@PA/BSA@NcadAb measured during 7 days of dispersion in the three different media. Data represent mean ± SD, n = 5.

as a chronic inflammatory disease.[22−24] Consequently, attenuation of inflammation has recently become an attractive strategy in the development of antiatherosclerotic therapies.[25,26] Among existing clinical trials, an IL-1β neutralizing antibody (i.e., CANTOS trial) has shown some promise to inhibit inflammation-induced EndoMT and slow the development of atherosclerosis.[27] However, suppressing systemic inflammation has its limitations, especially for patients with chronic diseases, considering that inflammation is essential for the host defense against invading pathogens and infections.[27,28] In summary, existing strategies aiming to block the cytokine regulatory pathways of EndoMT suffer from poor selectivity, unwanted side effects, and a heterogeneous response from endothelial cells with different origins. Notably, EndoMT inhibitors focus on preventing EndoMT, leaving the endothelial cells that have already undergone EndoMT unresolved.

In this study, we design a simple but powerful nanoparticle-based approach to target and modulate endothelial cell plasticity via driving the reversal of EndoMT (R-EndoMT, i.e., switching the mesenchymal phenotype back to the endothelial phenotype, Figure 1). This approach represents a

https://doi.org/10.1021/acsnano.3c12281
ACS Nano 2024, 18, 8229−8247

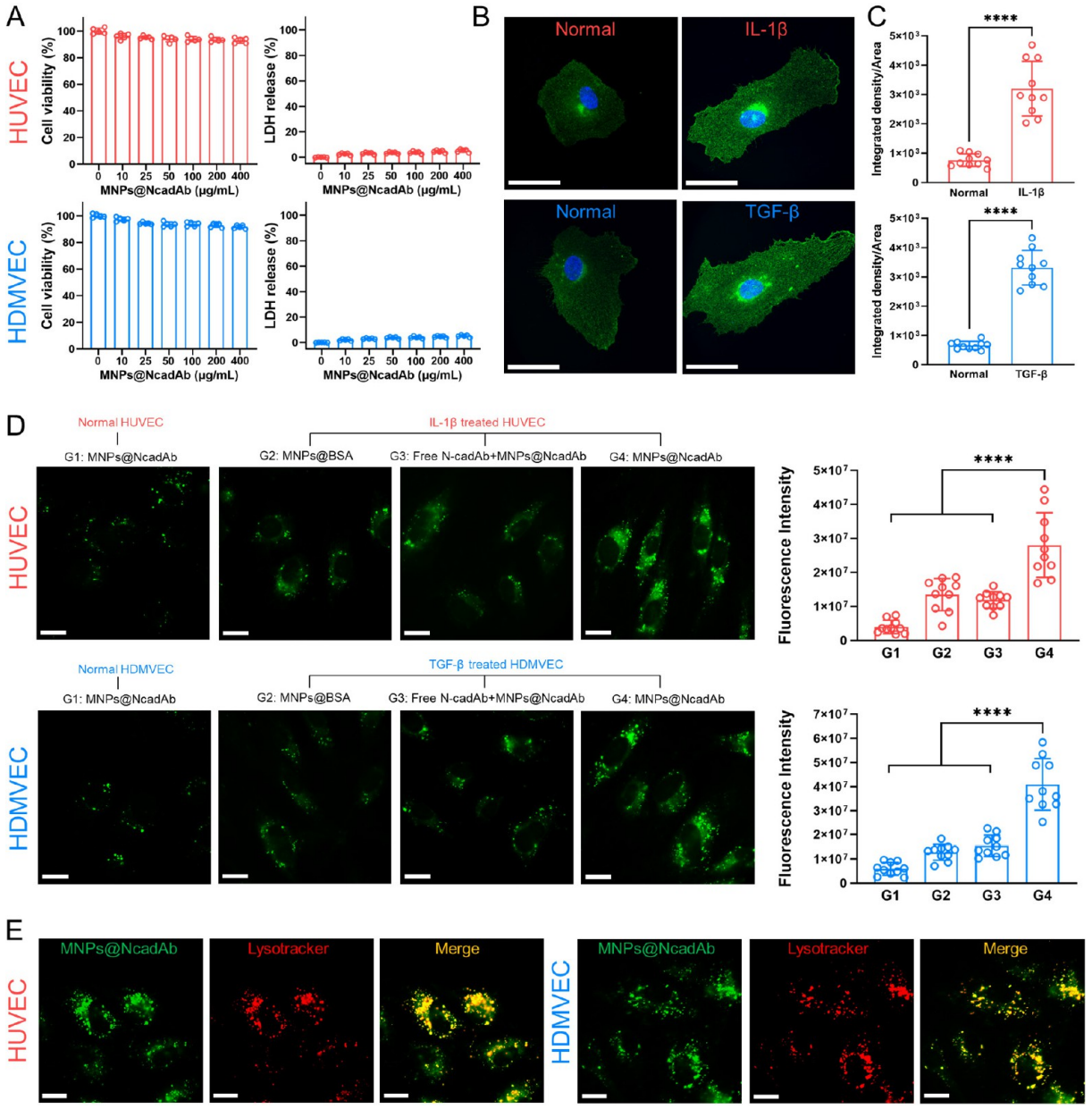

Figure 3. Endothelial cell compatibility and targeting ability of MNP@NcadAb. (A) XTT and LDH assays evaluating the viability and membrane damage of HUVEC and HDMVEC after incubation with different concentrations of MNP@NcadAb for 12 h. Data represent mean ± SD, n = 5. (B) Immunofluorescence staining of N-cadherin (green) on untreated (normal) HUVEC, IL-1β treated HUVEC, untreated (normal) HDMVEC, and TGF-β treated HDMVEC. Scale bars: 20 μm. (C) Statistical analysis of N-cadherin expression using the immunofluorescence images. Data represent mean ± SD, n = 10. (D) Fluorescence tracking and statistical analysis of cellular uptake of FITC-tagged MNP@NcadAb and MNP@BSA by normal and cytokine-activated HUVEC and HDMVEC. Scale bars: 20 μm. Total fluorescence intensity of individual cells is used to quantify the uptake of nanoparticles by cells. Data represent mean ± SD, n = 10. (E) Fluorescence colocalization (yellow) of FITC-tagged MNP@NcadAb (green) with lysosome (red) in IL-1β treated HUVEC and TGF-β treated HDMVEC. Scale bars: 20 μm. Statistical significance is determined by one-way ANOVA with Tukey's post hoc test. ****p < 0.0001.

significant deviation from existing approaches, which primarily focus on the inhibition of EndoMT. R-EndoMT here is achieved by targeting N-cadherin, a transmembrane marker specific to the endothelial-derived mesenchymal cells,[29,30] using N-cadherin antibody functionalized melanin nanoparticles. Of particular significance, we hypothesize that the N-cadherin targeted melanin nanoparticles serve a dual purpose: to specifically target the activated endothelium with overexpressed surface N-cadherin rather than normal endothelium and, furthermore, to modulate the downstream signaling of N-cadherin to reverse EndoMT. We demonstrate that this approach can be applied to reverse EndoMT (induced by IL-1β, TGF-β, and cancer cell-derived medium) in a wide range of vascular endothelial cells obtained from arteries, veins, and capillaries. This leads to a recovered endothelial barrier along with significantly reduced leukocyte and cancer cell trans-endothelial migration, which could potentially slow or stop atheromatous plaque formation and cancer cell extravasation in early stages (Figure 1). Finally, we reveal the molecular mechanism of R-EndoMT mediated by our nanoparticle system. Given the increasingly recognized implications of EndoMT in a variety of vascular and

https://doi.org/10.1021/acsnano.3c12281
ACS Nano 2024, 18, 8229−8247

nonvascular diseases including atherosclerosis, cancer, and organ fibrosis, our approach highlights a promising alternative to hinder the progression of these EndoMT-associated diseases.

RESULTS

Functionalization and Characterization of Natural Melanin Nanoparticles (MNPs). We selected natural MNPs over their synthetic analog (i.e., polydopamine NPs) in this work owing to their natural abundance, high surface area/volume ratio, good dispersibility, excellent cell and blood compatibility, well-understood surface chemistry, and facile surface functionalization.[31−33] The natural MNPs were extracted from food-grade cuttlefish ink using a sequential centrifugation method. To functionalize the MNPs with N-cadherin antibody, MNPs were premodified with a layer of protein A (PA) and bovine serum albumin (BSA) via a well-defined Michael addition and/or Schiff-base reaction between the -NH_2 moiety of PA/BSA and the o-quinones of melanin in a slightly alkaline medium (Figure 2A).[34] Here, PA serves as a linker to further graft N-cadherin antibody through its high affinity to the Fc region of immunoglobulin, while BSA acts as a spacer to adjust antibody density, as well as to resist nonspecific binding on the nanoparticle surface.[35,36] This design offers an optimal orientation of antibody on the nanoparticle surface with the antigen-binding Fab regions facing outward, and meanwhile, it avoids the crowding effect of Fab domains from adjacent antibodies.[37] Transmission electron microscope imaging showed an increased diameter of MNPs (from ∼128 to ∼136 nm) and a rougher nanoparticle surface after functionalization with the N-cadherin antibody (Figure 2B,C). The two-step surface functionalization was also verified through a gradually increased hydrodynamic diameter (Figure 2D) and zeta potential (Figure 2E) of MNPs in H_2O: Bare MNPs (179.3 nm, −22.7 mV), MNP@PA/BSA (190.9 nm, −18.6 mV), and MNP@PA/BSA@NcadAb (206.6 nm, −13.1 mV). The attachment of the antibody on the MNPs was further affirmed by scanning electron microscopy with energy dispersive X-ray spectroscopy (SEM/EDX) as the presence of sulfur was only found following the second step of functionalization owing to the disulfide bonds in immunoglobulins (Figures 2F, S1). Finally, the excellent colloidal stability of as-prepared N-cadherin antibody functionalized MNPs (i.e., MNP@PA/BSA@NcadAb, MNP@NcadAb in short) was evidenced by the unchanged absorbance spectrum and consistent hydrodynamic size when dispersed in three different media (including H_2O, PBS buffer, and serum-containing cell culture medium, Figure 2G,H) for 7 days, suggesting their potential dispersibility and stability in the blood circulation.

Endothelial Cell Compatibility and Targeting Ability of MNP@NcadAb. To investigate the effect of MNP@NcadAb on endothelial cells, we carefully chose two well-established primary cell lines, human umbilical vein endothelial cells (HUVEC) and human dermal microvascular endothelial cells (HDMVEC), as the models to represent macrovascular and microvascular endothelium, respectively. HUVEC, a typical macrovascular barrier, has been utilized as a classic endothelial model to study the development and treatment of atherosclerosis,[38] whereas HDMVEC, originating from capillary vessels, is suitable for evaluating cancer metastasis in the microvascular network.[39]

Endothelial cell compatibility of MNP@NcadAb was evaluated by two routinely used cytotoxicity assays including an XTT-based viability assay that measures cellular metabolic activity and an LDH-based cytotoxicity assay that quantifies leaked cytoplasmic LDH enzyme as an indicator of plasma membrane damage (Figure 3A). Assay results showed that MNP@NcadAb (as high as 400 μg/mL) had negligible effects on the metabolic activity and membrane integrity of both endothelial cell lines after 12 h of nanoparticle−cell co-incubation, suggesting the favorable endothelial cell compatibility of MNP@NcadAb. The assay results also defined the noncytotoxic range of MNP@NcadAb concentration used in the subsequent experiments. To examine the targeting ability of MNP@NcadAb to the activated endothelial cells instead of normal, quiescent endothelial cells, HUVEC were treated with IL-1β, a pro-inflammatory cytokine that triggers EndoMT and advances the development of atherosclerosis,[40] while the HDMVEC were activated by TGF-β, a well-known EndoMT inducer and contributor to cancer metastasis.[17] Immunofluorescence staining of N-cadherin indicated that both IL-1β and TGF-β treatments resulted in considerably higher expression of membrane N-cadherin (i.e., a typical mesenchymal marker) on the activated endothelial cells, in comparison to the normal, quiescent (inactivated) endothelial cells (Figures 3B,C, S2 and S3). The N-cadherin here appeared to show a diffused distribution on the cell surface, consistent with previous reports.[41,42] As expected, we then observed nearly 7 times higher uptake of fluorescence tagged MNP@NcadAb (100 μg/mL, after 12 h incubation with cells) by the activated HUVEC and HDMVEC (G4), as compared with their normal, quiescent counterparts (G1) (Figure 3D). The targeting specificity of MNP@NcadAb was also strengthened by two control groups (Figure 3D, G2 and G3): In comparison to the highest uptake groups (i.e., MNP@NcadAb with activated HUVEC and HDMVEC), ∼2−3 times lower uptake of nonspecific MNP@BSA was shown on both activated cell lines (G2), and ∼2−3 times lower uptake of MNP@NcadAb was observed on N-cadherin antibody pretreated, activated HUVEC and HDMVEC (namely, a competition or blocking assay, G3). Reproducible data on cellular uptake are shown in Figures S4 and S5. The internalization of MNP@NcadAb by activated endothelial cells was further revealed by a near-perfect overlap (yellow color) between the fluorescence tagged MNP@NcadAb (green color) and the Lysotracker (red color), suggesting that most MNP@NcadAb were cell-internalized and located within the lysosomes of endothelial cells (Figure 3E). Together, these results demonstrate the excellent endothelial cell compatibility of MNP@NcadAb, along with their specific targeting to activated endothelial cells with high expression of surface N-cadherin.

MNP@NcadAb Restores the Barrier Function of Cytokine-Activated Endothelium. The major function of vascular endothelial cells is to serve as a door keeper to restrict the transport of molecules and cells across this barrier layer. However, previous studies indicate that elevated cytokine levels (such as IL-1β and TGF-β) in blood circulation in response to certain pathological conditions can disrupt endothelial integrity and enhance endothelial permeability via triggering of the EndoMT process. The enhanced endothelial permeability then opens the paracellular route for trans-endothelial migration of immune and tumor cells to the underlying tissues, which is a crucial, early step for the development of atherosclerosis and cancer metastasis.[9,13] Thus, how to "close" the paracellular openings and find ways to recover the intactness and barrier function of vascular

https://doi.org/10.1021/acsnano.3c12281
ACS Nano 2024, 18, 8229−8247

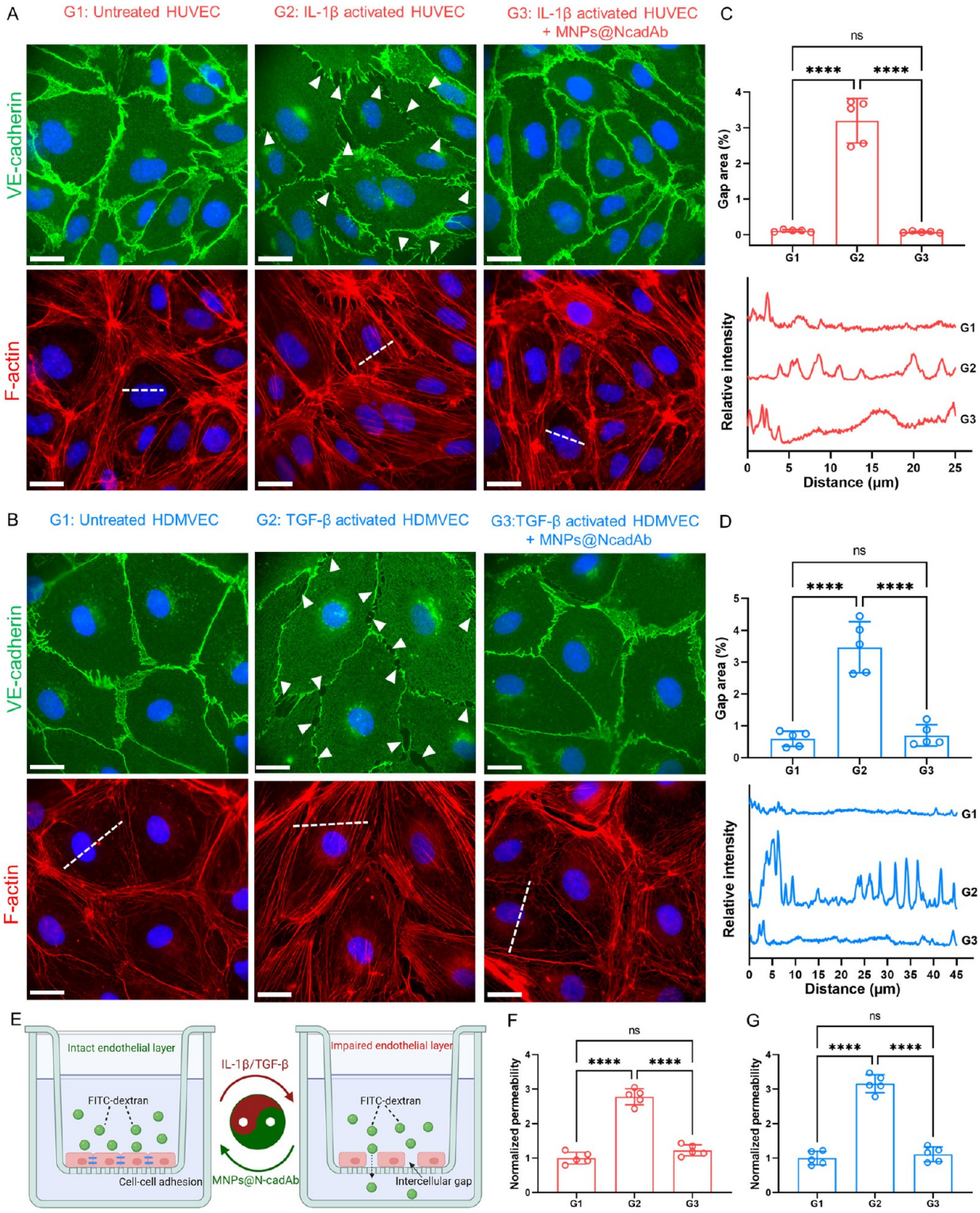

Figure 4. MNP@NcadAb restores the barrier function of cytokine activated endothelium. (A, B) Cofluorescence staining of VE-cadherin (green) and F-actin (red) on (A) HUVEC and (B) HDMVEC monolayers in different treatment groups. The cytokine induced intercellular gaps are marked by white triangles. White dashed lines are used to profile the actin stress fibers along the cell body. Scale bars: 20 μm. (C, D) Statistical analysis of gap area and profiles of actin stress fibers along the white dashed lines on (C) HUVEC and (D) HDMVEC monolayers. Data represent mean ± SD, n = 5. (E) Schematic illustration of endothelial permeability assay based on the transport of FITC-dextran across endothelial monolayers. (F, G) Statistical analysis of FITC-dextran transport across (F) HUVEC and (G) HDMVEC monolayers in different treatment groups. Data represent mean ± SD, n = 5. Statistical significance is determined by one-way ANOVA with Tukey's post hoc test. ****p < 0.0001.

endothelium will be the key to slow the progression of these diseases.

Since MNP@NcadAb has shown specific targeting to IL-1β and TGF-β activated endothelial cells, we next assessed the

https://doi.org/10.1021/acsnano.3c12281
ACS Nano 2024, 18, 8229−8247

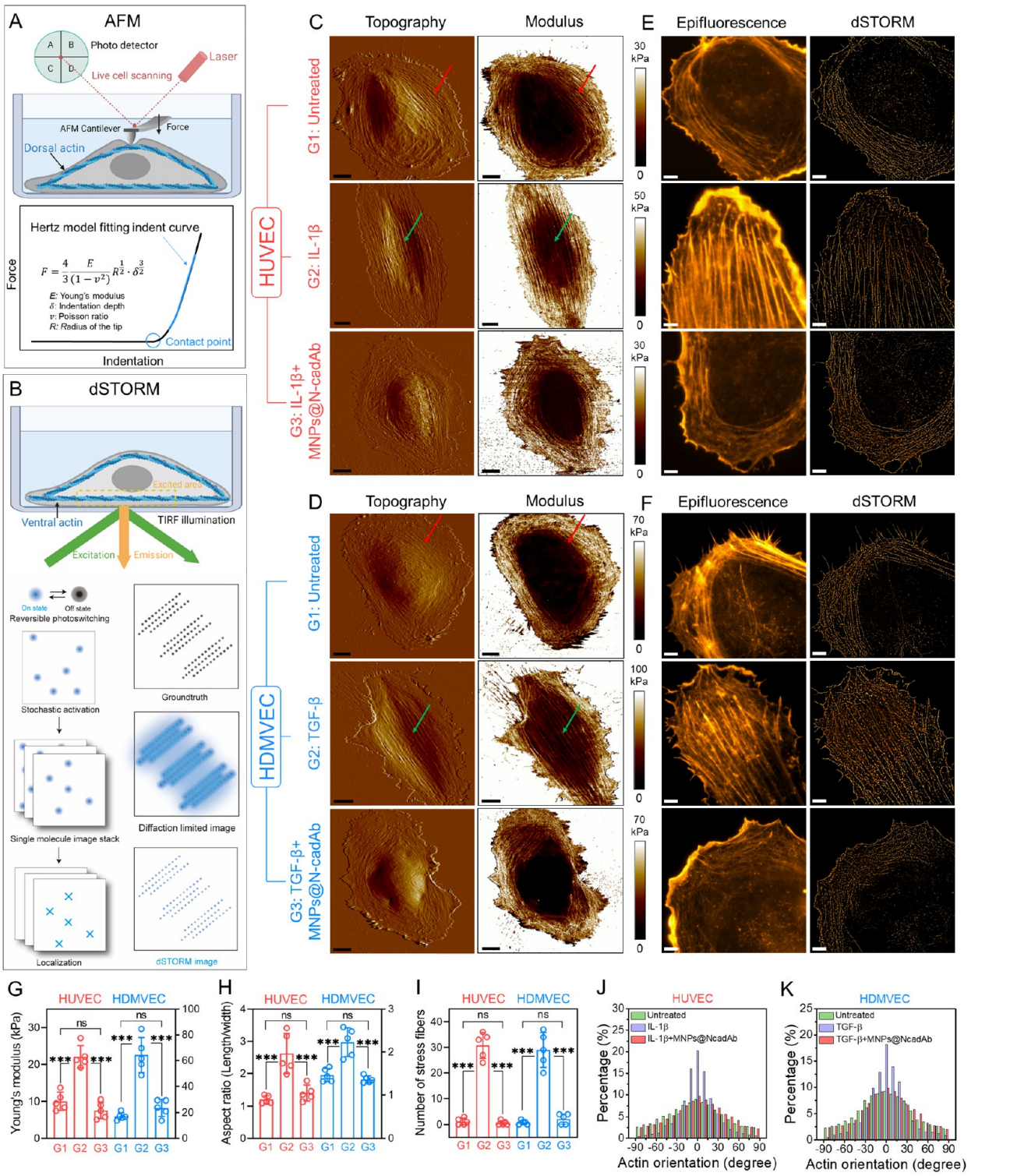

Figure 5. MNP@NcadAb reverses EndoMT at the single cell level. (A, B) Schematic illustration of the experimental setup for (A) AFM nanomechanical scanning of live cells and (B) the working principle of dSTORM imaging. (C, D) AFM nanomechanical imaging of single (C) HUVEC and (D) HDMVEC in different treatment groups. Left channel: Topography. Right channel: Young's modulus. Red arrows mark the circumferential actin belts and green arrows indicate the dorsal actin stress fibers. Scale bars: 10 μm. (E, F) dSTORM imaging of F-actin in single (E) HUVEC and (F) HDMVEC in different treatment groups. Left channel: Conventional epifluorescence images. Right channel: dSTORM images. Scale bars: 5 μm. (G, H) Statistical analysis of (G) average Young's modulus and (H) aspect ratio of individual cells based on AFM images. (I–K) Statistical analysis of (I) number of stress fibers and (J, K) actin orientation of individual cells based on dSTORM images. Data represent mean ± SD, n = 5. Statistical significance is determined by one-way ANOVA with Tukey's post hoc test. ***p < 0.001.

https://doi.org/10.1021/acsnano.3c12281
ACS Nano 2024, 18, 8229–8247

effect of MNP@NcadAb on the barrier function of activated endothelial monolayers. Through cofluorescence staining of an endothelial cell junction protein, VE-cadherin, and cytoskeletal F-actin (Figures 4A,B and S6−S11), it was clear to see that the untreated HUVEC and HDMVEC possessed an intact monolayer with continuous cell−cell adhesion and circumferential actin filaments lining the cell boundaries, both of which are typical features of normal, quiescent endothelial monolayers.[43] Here, the circumferential actin filaments along the cell boundary are known to be anchored by the transmembrane VE-cadherin, and they cooperate to stabilize the endothelial cell−cell contacts and barrier integrity.[44,45] IL-1β treated HUVEC and TGF-β treated HDMVEC monolayers manifested dramatic morphological changes, including discontinuous cell−cell adhesion, the appearance of intercellular gaps (marked by white triangles), and the increase of actin stress fibers along the cell body (cross-profiled by white dashed lines), indicating that IL-1β and TGF-β activation changed the endothelial morphology and impaired the endothelial integrity. Noticeably, the VE-cadherin amount significantly reduced around the gaps, suggesting that the disruption in cell−cell junctions could cause the formation of intercellular gaps. The actin stress fibers here are regarded as contractile, motile cytoskeletal structures that give rise to increased intracellular tension and cell mobility, also contributing to the disruption of endothelial integrity and barrier function.[46−49] Importantly, after treatment of the IL-1β activated HUVEC and the TGF-β activated HDMVEC monolayers with 100 μg/mL MNP@NcadAb for 12 h, both impaired endothelial layers were able to recover their original intactness and morphology without perceptible intercellular gaps and actin stress fibers. These visual examinations were supported by analyzing the intercellular gap areas and actin stress fiber numbers in three different groups (Figure 4C,D), among which the cytokine treated groups possessed the highest gap areas (~3%) and the most actin stress fibers, while the MNP@NcadAb treated groups and untreated groups both displayed significantly lower gap areas (~0.1−0.5%) and almost no actin stress fibers. To quantitatively validate the endothelial impairing effect of cytokines and recovering effect of MNP@NcadAb, we performed an endothelial permeability assay using FITC-dextran transport to measure the permeability of endothelial layers in different groups (Figure 4E). Through this assay, the concentration effect of cytokine activation and nanoparticle treatment on endothelial permeability can be systematically established (Figures S12 and S13). Consistent with the trends seen in gap area analysis, the cytokine treatments (5 ng/mL IL-1β, 10 ng/mL TGF-β, 12 h) resulted in an ~3-fold increase in the transport of FITC-dextran across the endothelial barriers, whereas further treatment of the impaired endothelial layers with MNP@NcadAb (100 μg/mL for 12 h) recovered the endothelial barriers and brought them back to their original permeability (Figure 4F,G). The permeability after recovery could be maintained for at least 72 h under normal culture conditions (Figure S14). Here, we also noted no impairing effect of MNP@NcadAb on the normal, quiescent endothelial monolayers (Figures S15 and S21), which is in line with the minimal cellular uptake of nanoparticles by these cells as demonstrated earlier. Likewise, due to the lower cellular uptake of nonspecific MNP@BSA by cytokine-activated endothelial cells and MNP@NcadAb by cytokine-activated endothelial cells pretreated with an endocytosis inhibitor (methyl-β-cyclodextrin), the impaired endothelial monolayers cannot be reversed/healed (Figure S16). Therefore, these results suggest the importance of the endocytosis of MNP@NcadAb.

To further ascertain the recovery effect of MNP@NcadAb, two control experiments were employed using N-cadherin antibody functionalized gold nanorods and free N-cadherin antibody, with antibody amounts equivalent to the MNP@NcadAb (calculated in Supporting Information), to treat cytokine-activated endothelial cells (Figures S17, S18, and S21). Normal culture medium served as a negative control (Figures S19 and S21). The monolayer morphology and permeability assay results showed that N-cadherin antibody functionalized gold nanorods had a similar endothelial recovery effect with the MNP@NcadAb treatment, whereas free N-cadherin antibody just manifested a modest recovery effect on the impaired monolayers, which could be attributed to the multivalency effect of antibodies on the nanoparticle surface. As expected, the normal culture medium had almost no recovery effect on the impaired monolayers, suggesting that these monolayers, once activated by cytokines, cannot "heal" by themselves in the given period of time (12 h). Furthermore, we demonstrated that MNP@NcadAb treatment was able to restore the morphology and barrier function of activated endothelial layers in the presence of cytokines (Figures S20 and S21), which suggested the robustness of this approach in treating extreme harsh conditions (i.e., when the sustained endothelial exposure to elevated cytokines was present). Collectively, these data provide compelling evidence that MNP@NcadAb treatment can restore the morphology and barrier function of cytokine-activated, integrity-impaired endothelium.

MNP@NcadAb Reverses EndoMT at the Cellular and Molecular Levels. As we observed the morphological change of endothelial monolayers in response to the cytokine activation and MNP@NcadAb treatment, we next questioned whether these changes on the monolayers can be attributed to the EndoMT program of individual endothelial cells, given the important roles of cytokine activation and N-cadherin expression in endothelial cell phenotypical plasticity.

Therefore, to better characterize the phenotypical changes of individual endothelial cells, we utilized atomic force microscopy (AFM) to image single cells in different experimental groups. Specifically, AFM nanomechanical mode was performed to investigate the morphology and mechanical properties of live cells in a liquid environment (Figure 5A). During nanomechanical scanning, a spherical tip probes the cell surface with an applied force and a force−indentation curve is collected, and then the local Young's modulus is calculated from this curve using the Hertz model.[50,51] The generated modulus map of a single cell offers a simple, vivid way to resolve the actin filaments residing in the dorsal layer of the cell since these actin structures are the main contributors to the cell rigidity.[52−54] As depicted in Figures 5C,D and S22−S27, the topography and modulus channels showed excellent correlations in terms of cell topography and the locations of dorsal actin. In particular, both channels exhibited well-grooved patterns with appreciable colocalization between the topography and modulus, suggesting the presence of actin filaments underneath the plasma membrane. The untreated HUVEC and HDMVEC displayed a round, cobblestone-like cell shape featuring a flat, thin membrane and underlying circumferential actin belts surrounding the entire cell boundary (marked by red arrows). In contrast, IL-1β activated HUVEC and TGF-β activated HDMVEC changed to a spindle-like

https://doi.org/10.1021/acsnano.3c12281
ACS Nano 2024, 18, 8229−8247

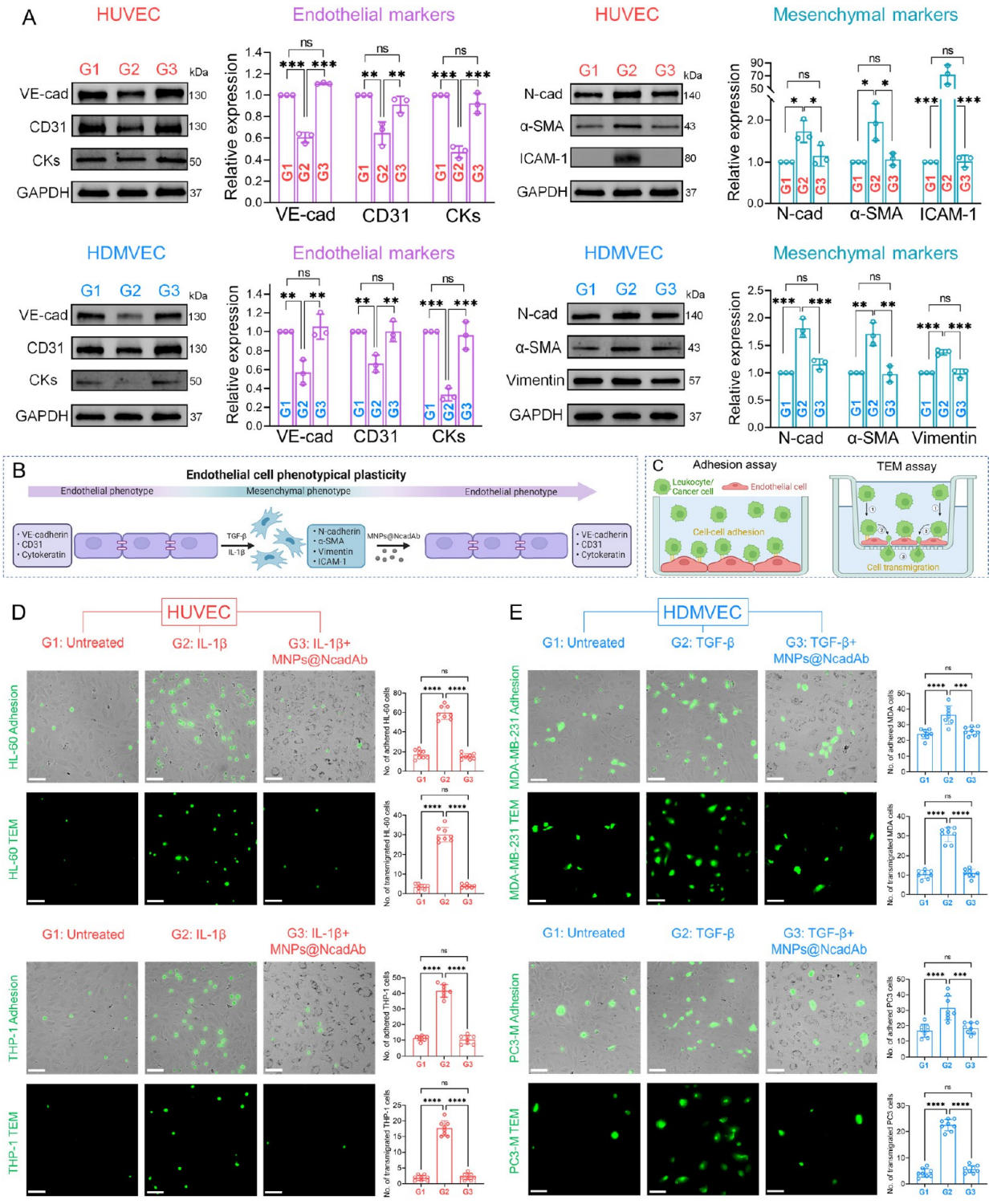

Figure 6. Protein markers of endothelial phenotypical transition, endothelial adhesion, and trans-endothelial migration (TEM) of leukocytes and cancer cells. (A) Western blotting analysis of endothelial and mesenchymal protein markers of HUVEC and HDMVEC in different treatment groups. G1: Untreated, normal endothelial cells. G2: Cytokine activated endothelial cells. G3: Cytokine activated endothelial cells followed by MNP@NcadAb treatment. GAPDH serves as a house-keeping marker. Data represent mean ± SD, n = 3. (B) Schematic illustration of elevated protein markers due to the cytokine activation and MNP@NcadAb treatment. (C) Working principles of endothelial adhesion and TEM assays of leukocytes and cancer cells. (D) Endothelial adhesion and TEM of leukocytes (HL-60 and THP-1) on/across HUVEC monolayers in different treatment groups and their statistical analysis. (E) Endothelial adhesion and TEM of cancer cells (MDA-MB-231 and PC3-M) on/across HDMVEC monolayers in different treatment groups and their statistical analysis. Scale bars: 100 μm. Data represent mean ± SD, n = 8. Statistical significance is determined by one-way ANOVA with Tukey's post hoc test. ****p < 0.0001, ***p < 0.001, **p < 0.01, and *p < 0.05.

https://doi.org/10.1021/acsnano.3c12281
ACS Nano 2024, 18, 8229−8247

morphology with dorsal actin stress fibers parallelly running along the cell body (pointed out by green arrows). Here, these morphological changes are in good agreement with the typical characteristics of endothelial phenotype (i.e., cobblestone-like cell shape, rich in circumferential actin belts) and mesenchymal phenotype (i.e., spindle-like cell shape, rich in actin stress fibers) of endothelial cells,[4] suggesting the occurrence of endothelial−mesenchymal transition of HUVEC and HDMVEC in response to the cytokine activation. Importantly, the MNP@NcadAb treatment was able to convert the mesenchymal-like HUVEC and HDMVEC back to their original morphology, as evident from the disappearance of dorsal stress fibers and spindle cell shape, accompanied by the reappearance of circumferential actin belts and circular cell shape. These visual observations on AFM images were further reinforced by analyzing the average Young's modulus and aspect ratio of individual cells (Figure 5G,H). Among the three experimental groups, the cytokine-activated endothelial cells showed the highest aspect ratio (∼2−2.5) in cell shape and the highest average Young's modulus on the cellular central region (∼20−60 kPa) owing to the presence of dorsal stress fibers, whereas both untreated and MNP@NcadAb treated groups displayed a lower aspect ratio of ∼1−1.2 and an average Young's modulus of ∼8−20 kPa due to the lack of dorsal stress fibers.

To further validate the phenotypical change of individual endothelial cells, a super-resolution imaging technique, direct stochastic optical reconstruction microscopy (dSTORM), was performed to image the actin filaments within single cells. Compared to the conventional epifluorescence illumination, dSTORM here operates in a total internal reflection illumination mode to excite a thin layer (∼0.2 μm) above the imaging substrate and rejects background fluorescence (Figure 5B). Thus, dSTORM complements the AFM, resolving the ventral actin filaments inaccessible to the AFM by imaging fluorescence from actin-binding fluorophores near the coverslip surface. During the dSTORM imaging, the individual fluorophores were stochastically activated and localized in each image frame; the final super-resolution images were reconstructed by stacking thousands of image frames with the activated fluorophores and their localizations.[55−57] As shown in Figures 5E,F and S28−S33, the dSTORM images in three experimental groups showed results consistent with the AFM images, among which the cytokine-activated endothelial cells displayed the most ventral stress fibers parallel with the cellular long axis, whereas the other two groups exhibited similar circumferential actin belts and a lack of ventral stress fibers. The high spatial resolution of dSTORM images also allowed for the statistical analysis of stress fiber numbers and actin orientations (Figure 5I−K), which further substantiated the phenotypical transition of endothelial cells in different experimental groups. These imaging data suggest that cytokine activation causes EndoMT in individual endothelial cells and, more importantly, the MNP@NcadAb treatment can reverse the activated, mesenchymal-like endothelial cells back to their initial endothelial phenotype.

Apart from the cellular level investigation, we also examined the effect of MNP@NcadAb on cytokine-activated endothelial cells at the molecular level. Western blotting was utilized to analyze a panel of endothelial and mesenchymal protein markers in endothelial cells, including platelet endothelial cell adhesion molecule-1 (CD31), VE-cadherin, and cytokeratin as endothelial markers and intercellular adhesion molecule-1 (ICAM-1), N-cadherin, alpha-smooth muscle actin (α-SMA), and vimentin as mesenchymal makers (Figure 6A). Herein, besides the common protein markers shared by macrovascular and microvascular endothelial cells, ICAM-1 is a typical mesenchymal marker for macrovascular endothelial cells (HUVEC) in response to inflammatory cytokines (e.g., IL-1β),[21] whereas vimentin serves as a mesenchymal maker for microvascular endothelial cells (HDMVEC) in response to TGF-β.[58] Our immunoblotting and its semiquantitative analysis showed that cytokine activation resulted in the downregulation of endothelial markers, including CD31, VE-cadherin, and cytokeratin, in both cell lines, along with the upregulation of mesenchymal markers, including ICAM-1 in HUVEC, vimentin in HDMVEC, and N-cadherin and α-SMA in both cell lines, suggesting that cytokine activation induced EndoMT in both endothelial cells at the molecular level. Importantly, after treatment of the activated endothelial cells with MNP@NcadAb, all protein markers we tested here returned to their original levels prior to the cytokine activation, indicating the reversal of EndoMT in both endothelial cells at the molecular level (Figure 6A,B). These results are in line with our prior observations on endothelial monolayers, where the upregulation of VE-cadherin induced by MNP@NcadAb treatment re-established the endothelial cell−cell adhesion and barrier function and the downregulation of contractile cytoskeletal proteins including α-SMA and vimentin reduced the intracellular tension, also contributing to the recovery of endothelial intactness. Together, these single-cell imaging and immunoblotting data demonstrate that MNP@NcadAb treatment is able to reverse cytokine-activated EndoMT in endothelial cells, observable at both cellular and molecular levels, and these phenotypical changes in individual cells promote the recovery of the endothelial monolayer and the restoration of its barrier function.

R-EndoMT Attenuates Endothelial Adhesion and Trans-Endothelial Migration of Leukocytes and Cancer Cells. It has been documented that macrovascular endothelial cells activated by inflammatory cytokines (e.g., IL-1β) overexpress cell adhesion molecules including ICAM-1 and VCAM-1, facilitating the recruitment and adhesion of inflammatory-related leukocytes such as monocytes and neutrophils onto endothelial cells.[8] In the context of cancer metastasis within microvasculature, endothelial cells in response to TGF-β activation upregulate surface N-cadherin, which promotes N-cadherin mediated homophilic adhesion between endothelial cells and N-cadherin-expressing cancer cells.[13] Following the initial adhesion, adhered leukocytes or cancer cells can exploit the enhanced endothelial permeability to cross the compromised endothelial barriers, which initiates atherosclerotic plaque formation and cancer metastasis.[10,17] With these considerations along with our monolayer and immunoblotting data, we would expect that MNP@NcadAb mediated R-EndoMT would not only attenuate the endothelial adhesion of leukocytes and cancer cells by downregulating the key adhesion molecules (i.e., ICAM-1, N-cadherin) but also recover the compromised endothelial barriers by closing the intercellular gaps; both factors would hinder the trans-endothelial migration of leukocytes and cancer cells to the underlying tissues.

Therefore, we subsequently evaluated the effect of MNP@NcadAb on the endothelial adhesion and trans-endothelial migration (TEM) of leukocytes and cancer cells using two well-established endothelial cell assays, as illustrated in Figure

https://doi.org/10.1021/acsnano.3c12281
ACS Nano 2024, 18, 8229−8247

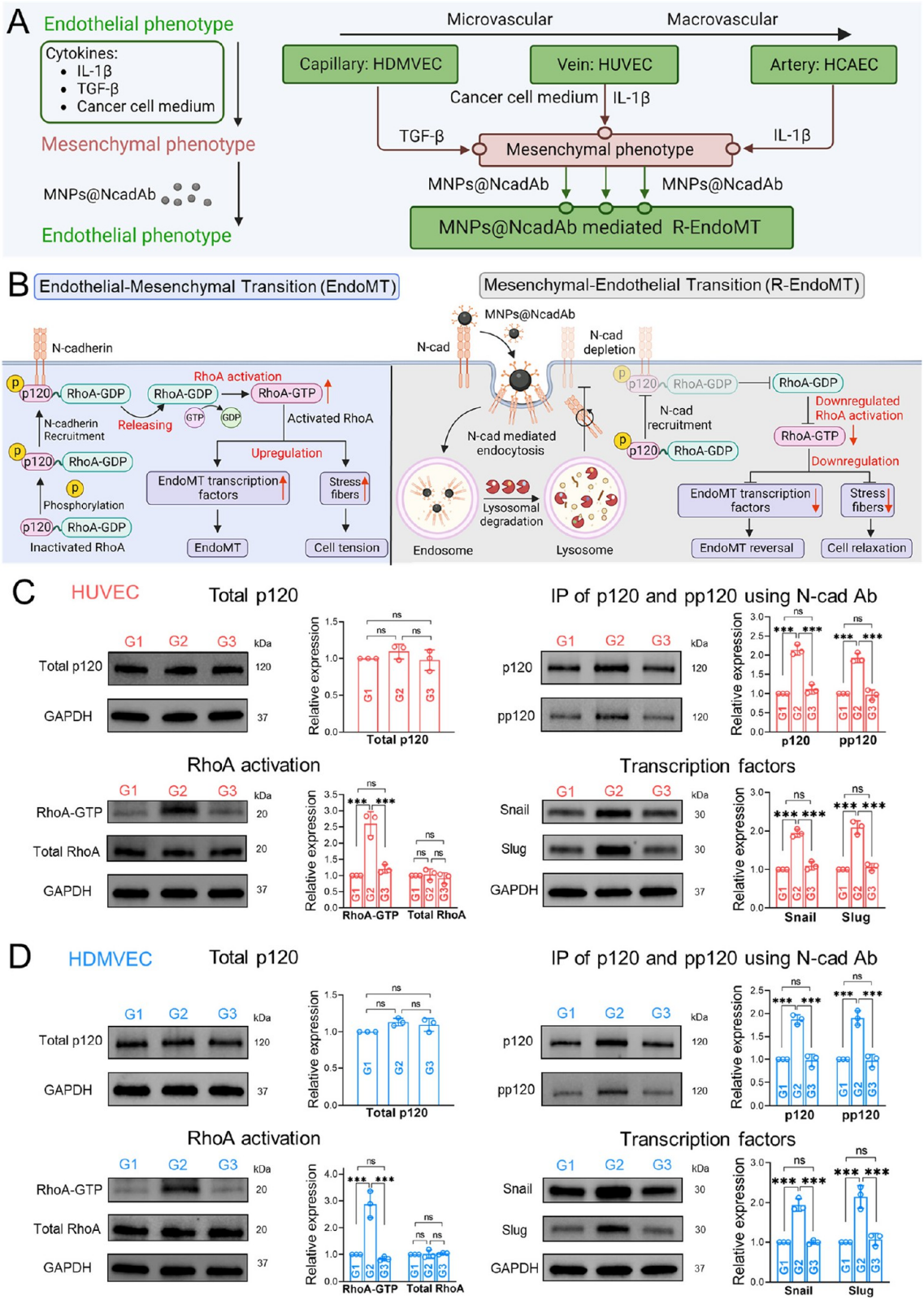

Figure 7. Applicability and molecular mechanism of MNP@NcadAb mediated R-EndoMT. (A) Diagram summarizing the broad applicability of MNP@NcadAb mediated R-EndoMT in various types of endothelial cells activated by a diverse range of cytokines. (B) Proposed molecular mechanism of N-cadherin dependent EndoMT (left panel) and MNP@NcadAb mediated R-EndoMT (right panel). (C, D) Western blotting analysis of total p120 catenin, anti-N-cadherin antibody immunoprecipitated (IP) p120 catenin, and its tyrosine phosphorylation (pp120), RhoA activation, and transcription factors Snail and Slug in (C) HUVEC and (D) HDMVEC in different treatment groups. G1: Untreated, normal endothelial cells. G2: Cytokine activated endothelial cells. G3: Cytokine activated endothelial cells followed by MNP@NcadAb treatment. GAPDH serves as a house-keeping marker. Data represent mean ± SD, $n = 3$. Statistical significance is determined by one-way ANOVA with Tukey's post hoc test. ***$p < 0.001$.

https://doi.org/10.1021/acsnano.3c12281
ACS Nano 2024, 18, 8229−8247

6C. As shown in the adhesion assays, the adhesion of two inflammatory-related leukocytes including a human promyelocytic leukemia cell line (differentiated HL-60) and a human monocytic leukemia cell line (THP-1) to the IL-1β activated HUVEC significantly increased (~4-fold) compared to that on untreated, quiescent HUVEC (Figure 6D). Likewise, the adhesion of two N-cadherin-expressing cancer cells, including a human breast cancer cell line (MDA-MB-231) and a prostate cancer cell line (PC3-M) to the TGF-β activated HDMVEC also increased (~1.5−2-fold) compared to that on untreated, quiescent HDMVEC (Figure 6E). Notably, MNP@NcadAb treatment on both activated endothelial cells was able to reduce the endothelial adhesion of leukocytes and cancer cells to their original levels on the untreated, quiescent endothelial cells (Figures 6D,E and S34−S37). The adhesion results are in accordance with our immunoblotting data for ICAM-1 and N-cadherin in each treatment group. The same trends were also observed in the TEM assays, among which cytokine-activated endothelial cells allowed the highest TEM of leukocytes and cancer cells, and MNP@NcadAb treatment on activated endothelial cells was able to decrease the TEM of leukocytes and cancer cells to levels comparable to untreated, quiescent endothelial cells (Figures 6D,E and S38−S41). Here, it should be noted that the decrease in leukocytes and cancer cells observed in TEM assays not only results from the reduced endothelial adhesion but also is attributable to the recovered endothelial barriers with minimal intercellular gaps. This notion is supported by calculating the percentage of trans-migrated cells within the adhered cells (Figure S42). The cytokine-activated groups allowed ~40−50% of adhered leukocytes and ~70−80% of adhered cancer cells to trans-migrate across their respective endothelial barriers, whereas untreated and MNP@NcadAb treated groups permitted only ~20% of adhered leukocytes and ~30−40% of adhered cancer cells to transmigrate, owing to the significantly reduced intercellular gaps. Together, the adhesion and TEM assays confirm that MNP@NcadAb mediated R-EndoMT attenuates the endothelial adhesion and trans-endothelial migration of leukocytes and cancer cells, which could potentially prevent plaque and micrometastasis formation at the very early stages of atherosclerosis and cancer.

In addition to the trans-endothelial migration of leukocytes and cancer cells, we also assessed the migration ability of endothelial cells themselves (Figure S43). Previous studies suggested that endothelial-derived mesenchymal cells possess high mobility and invasiveness, which promotes their migration to underlying tissues, serving as a source of plaque-associated fibroblast-like cells and cancer-associated fibroblasts.[9,59] Our migration assays showed that both cytokine-activated endothelial cells manifested the highest migration among the three treatment groups, in line with their mesenchymal phenotype, whereas the other two groups displayed only modest migration, suggesting that MNP@NcadAb mediated R-EndoMT reduces the migration ability of cytokine-activated endothelial cells. Therefore, the MNP@NcadAb mediated R-EndoMT demonstrated here could also slow the progression of atherosclerosis and cancer by depleting their respective endothelial-derived fibroblast sources.

The results discussed thus far show the recovery effect of MNP@NcadAb treatment on IL-1β activated HUVEC (as a macrovascular model) and TGF-β activated HDMVEC (as a microvascular model). Considering that EndoMT in the context of atherosclerosis involves arterial (rather than venous) endothelial cells and considering the complexity of tumor microenvironments (i.e., multiple cytokines from cancer cells that could cause EndoMT),[17,60] we further extended our experiments to IL-1β activated human coronary artery endothelial cells (HCAEC) and cancer-cell conditioned medium activated HUVEC. This enabled us to evaluate the effect of MNP@NcadAb treatment on the whole spectrum of endothelial cells from capillaries, veins, and arteries activated by a diverse range of cytokines, as summarized in Figure 7A. As shown in Figures S44−S45, the monolayer morphology and permeability data, together with adhesion and TEM assay results, demonstrate that MNP@NcadAb treatment is also able to restore these endothelial barriers and attenuate the endothelial adhesion and trans-endothelial migration of leukocytes and cancer cells, suggesting the broad applicability of this approach in treating various types of endothelial cells, regardless of which cytokines are present.

Molecular Mechanism of MNP@NcadAb Mediated R-EndoMT. Our collective data suggest that MNP@NcadAb treatment reverses cytokine activated EndoMT in a broad range of endothelial cell types, and the recovered endothelial barriers attenuate the adhesion and transmigration of leukocytes and cancer cells, which could potentially slow the progression of atherosclerotic plaque formation and cancer metastasis. However, to fully translate MNP@NcadAb mediated R-EndoMT to treat various EndoMT-related diseases, understanding the underlying mechanism of R-EndoMT and the applicability of the mechanism in different cell types is of paramount importance. Thus, we finally turned our attention to the molecular mechanism of how MNP@NcadAb reversed EndoMT in activated endothelial cells. Previous studies suggested a major role of N-cadherin mediated signaling in the activation of RhoA,[61,62] a member of Rho family GTPases that positively regulates stress fiber formation and EMT-favoring transcription factors such as Snail and Slug in cancer cells during the EMT process.[37,50,63] The N-cadherin dependent RhoA activation was proposed to occur through the following mechanism (Figure 7B, left): Membrane N-cadherin recruits p120 catenin to form the N-cadherin/p120 membrane complex, which frees up RhoA from its inactive GDP bound state with p120, allowing local RhoA activation to RhoA−GTP near the plasma membrane. When not bound to N-cadherin, p120 catenin acts as a Rho inhibitor by directly binding to RhoA-GDP and suppresses RhoA activation.[64,65] Events like tyrosine phosphorylation of p120 causes a closer binding of p120 to N-cadherin, thus reducing the affinity of N-cadherin-associated p120 to RhoA-GDP and releasing the RhoA-GDP available for further activation.[66,67] However, whether the N-cadherin in the activated endothelial cells is adopting a role similar to that in cancer cells remains to be verified. It is also unknown if endothelial cells from different origins (i.e., microvascular vs macrovascular) would exert a common or different mechanism for R-EndoMT. In view of these considerations, we formed our mechanistic hypothesis for the MNP@NcadAb mediated R-EndoMT (Figure 7B, right): The uptake of MNP@NcadAb by activated endothelial cells would deplete the membrane of N-cadherin, which would hinder the N-cadherin recruitment of the RhoA inhibitor, p120. As a result, the RhoA activation would be downregulated along with its downstream EndoMT-related effectors, thus leading to R-EndoMT.

To test this hypothesis, we first examined the overall protein levels of p120 catenin by the immunoblotting of p120 in total

https://doi.org/10.1021/acsnano.3c12281
ACS Nano 2024, 18, 8229−8247

cell lysates. We noticed no significant difference in the overall levels of p120 catenin among different experimental groups in both cell lines (Figure 7C,D). Given that the interaction of membrane N-cadherin and p120 serves a key role in the RhoA activation, the total cell lysates were immunoprecipitated using anti-N-cadherin antibody and probed for p120 catenin and its tyrosine phosphorylation (pp120) using Western blots. Interestingly, the immunoprecipitated p120 catenin and its tyrosine phosphorylation displayed a similar trend as N-cadherin levels (Figure 6A) among different groups in both cell lines: The cytokine-activated groups exhibited the highest levels of p120 catenin and its tyrosine phosphorylation, while untreated and MNP@NcadAb treated groups showed similar, lower levels of p120 catenin and its tyrosine phosphorylation (Figure 7C,D). Since N-cadherin primarily presents in the cell membrane rather than the cytosol, these results confirmed the molecular interaction between N-cadherin and tyrosine phosphorylated p120 catenin on the cell membrane, and this membrane complex was expected to promote the RhoA activation near the plasma membrane. Hence, we next quantified the RhoA activation levels among different groups by measuring RhoA−GTP using an active RhoA pull-down assay. Consistent with the trends observed in the membrane N-cadherin and the trends of immunoprecipitated p120 catenin and its tyrosine phosphorylation levels, cytokine-activated groups in both cell lines also showed the highest RhoA−GTP levels, whereas the other two groups only possessed comparable, basal levels of RhoA activation (Figure 7C,D). Essentially, these data establish a strong correlation among membrane N-cadherin, tyrosine phosphorylated p120 catenin, and RhoA activation. As a membrane anchor for RhoA activation, N-cadherin governs the downstream pathway for RhoA activation, whereas the endocytosis of MNP@NcadAb by activated endothelial cells could deplete the membrane N-cadherin to the lysosomal degradation pathway (demonstrated via fluorescence colocalization images), thereby leading to the downregulation of RhoA activation. Based on these analyses, we further validated the downstream effectors of RhoA activation. Our previous studies on cancer EMT demonstrated that the downregulation of RhoA activation could lower its downstream EMT-favoring transcription factors (Snail and Slug proteins), which led to the restored epithelial phenotype of cancer cells.[37,50] Considering that EndoMT and EMT may share common transcription factors, we evaluated the levels of Snail and Slug transcription factors in both endothelial cells using Western blots. The results showed that Snail and Slug both followed a similar trend as RhoA activation, among which the cytokine-activated groups possessed the highest levels of Snail and Slug, whereas MNP@NcadAb treatment managed to reduce their amounts to basal levels (Figure 7C,D). As with EMT in cancer cells, the downregulation of Snail and Slug transcription factors could drive the phenotypical transition of endothelial-derived mesenchymal-like cells to return to their original endothelial phenotype. Taken together, these molecular-level studies dissect the N-cadherin dependent EndoMT mechanism of endothelial cells in response to cytokine activation and, more importantly, the N-cadherin dependent R-EndoMT mechanism induced by MNP@NcadAb treatment in both macrovascular and microvascular endothelial cells. That is by targeting and downregulating N-cadherin on activated, mesenchymal-like endothelial cells, MNP@NcadAb treatment downregulates the key proteins of the N-cadherin pathway, especially RhoA−GTP and its downstream effectors, including EndoMT-favoring transcription factors and stress fiber formation. The downregulation of EndoMT-favoring transcription factors (Snail and Slug) and stress fibers finally leads to R-EndoMT and recovered endothelial barriers (Figure 7B).

DISCUSSION

Atherosclerosis and cancer are, at first glance, two distinct diseases with quite different pathological mechanisms. However, the concept of EndoMT established in recent years has found a common ground between these diseases owing to the implications of EndoMT during the early development of atherosclerotic plaques and cancer metastases. In both cases, elevated levels of cytokines in the blood cause phenotypical changes in vascular endothelial cells (i.e., EndoMT) and thus disrupt the quiescence and intactness of endothelial barriers. The endothelial cells after EndoMT are typified by a high expression of cell adhesion molecules to recruit immune cells or cancer cells, and enhanced endothelial permeability further allows the attached immune or cancer cells to cross the impaired endothelial barrier, initiating plaque buildup or micrometastasis of cancer cells. Given these aspects of EndoMT, there should be two logical ways to slow the plaque buildup or micrometastasis of cancer cells: One approach is to hinder the interactions between immune or cancer cells with endothelial cells by blocking or down-regulating the cell adhesion molecules,[25,26] whereas the other approach is to "close" the intercellular gaps on the endothelium to stop the trans-endothelial migration of immune or cancer cells.[68] In our work, N-cadherin targeted MNPs are capable of reducing the adhesion between immune or cancer cells and endothelial cells and recovering the intactness of endothelial barriers by reversing EndoMT in endothelial cells. The synergistic effect of MNP@NcadAb is well aligned with the dual role of N-cadherin which not only serves as a cell adhesion molecule and mesenchymal marker but also acts as a transmembrane signaling molecule that regulates EndoMT. Indeed, the potential of this work goes far beyond atherosclerosis and cancer treatments considering the importance of EndoMT in the development of organ fibrosis and the prevalence of N-cadherin on various endothelial-derived mesenchymal cells.[3,69−71] As such, future work will focus on validating this approach in the context of reversing organ fibrosis. Apart from cytokine-induced EndoMT, another interesting area to investigate will be the effect of melanin/polydopamine NPs on reactive oxygen species (ROS) induced EndoMT given the ROS scavenging property of melanin/polydopamine NPs.[72]

The interaction of nanoparticles and endothelial cells has been increasingly under scrutiny since the endothelium lies in direct contact with nanoparticles in the blood circulation, regardless of whether the nanoparticles are intentionally injected for medical purposes or unintentionally introduced due to undesired exposure. Under most circumstances, the exposure of endothelial cells to nanoparticles can exert dose-dependent detrimental effects on the endothelium and further lead to other unwanted pathological outcomes. For instance, an extensive body of research from Leong's group highlighted that nanoparticle-induced endothelial leakiness (i.e., abbreviated as NanoEL) can promote cancer cell intravasation and extravasation due to the interaction of nanoparticles with endothelial junction proteins, causing increased intercellular gaps in the microvascular endothelial barriers that can be

https://doi.org/10.1021/acsnano.3c12281
ACS Nano 2024, 18, 8229−8247

exploited by the migrating cancer cells.[39,73] Interestingly, a recent work from the same group utilized NanoEL to increase tumor accessibility of anticancer drugs, which turned NanoEL to a beneficial effect.[74] Other studies also indicated that nanoparticles from air pollution and daily contact could mediate atherosclerosis progression by disrupting the plasma membrane of macrovascular endothelial cells.[75,76] In contrast, our work here shows that nanoparticles with a rational design can have a recovery or "healing" effect on an already impaired endothelium by reversing EndoMT of endothelial cells, which represents a completely opposite direction to the existing research. In addition, previous studies reported discrepancies in the response of the endothelium to nanoparticles or EndoMT inhibitors attributed to the structural and functional heterogeneity of the endothelium from different origins,[21,77] whereas the nanoparticle system in our work shows universal recovery effects on various organotypic endothelial cells from varied origins (artery, vein, and small capillary), independent of the activating cytokine involved, which implies that broad applicability and effectiveness of this approach in treating various vascular and nonvascular diseases may be possible. From a practical point of view, this work suggests that it may not be necessary to confine the antimetastatic or antiatherosclerotic therapy to targeting cancer or immune cells alone,[78] since the endothelium itself serves an ideal target for nanoparticle-based therapy. The easy access of nanoparticles to endothelial cells[79,80] and the simple but powerful design of the nanoparticle system discussed here will be beneficial for the translation of this approach to clinical practice.

CONCLUSIONS

In summary, we have demonstrated that N-cadherin antibody functionalized melanin nanoparticles (i.e., MNP@NcadAb) can target cytokine-activated, mesenchymal-like endothelial cells and drive their phenotypical transition from the mesenchymal phenotype back to the original endothelial phenotype, leading to a reversed EndoMT process, termed R-EndoMT. The MNP@NcadAb mediated R-EndoMT was validated at both cellular and molecular levels. Such phenotypical changes in endothelial cells led to recovered quiescence and intactness of endothelial barriers with significantly reduced leukocyte and cancer cell adhesion and transmigration, which could potentially stop atheromatous plaque formation and cancer metastasis in their early stages. This approach was shown to be applicable to recover the cytokine-compromised endothelial barriers from different origins spanning arteries, veins, and capillaries, independent of the activating cytokines involved. The underlying molecular mechanism of R-EndoMT was based on the modulation of an N-cadherin dependent RhoA activation pathway by MNP@NcadAb. Considering the growing implications of EndoMT in a variety of vascular and nonvascular diseases including atherosclerosis, cancer, and organ fibrosis, we expect this approach will provide an alternative solution to treat EndoMT-associated diseases by recovering and reinforcing endothelial barriers.

METHODS

Preparation and Surface Functionalization of MNPs. Cuttlefish ink was purchased from Amazon (Vendor: Marky's Cuttlefish Squid Ink from Spain). The MNPs were isolated from the cuttlefish ink by a sequential centrifugation approach: First, 5 g of cuttlefish ink was dispersed in 50 mL of deionized water with 1× TBS Tween-20 (28360, Thermo Fisher Scientific) and stirred for 4 h. The suspension was then centrifuged at 2000 rpm for 5 min to eliminate the largest particles. Next, the supernatant was centrifugated for 5 min at 7000 rpm to eliminate medium-size particles. Finally, the supernatant was centrifugated at 12000 rpm for 10 min to collect the desired MNPs, and these MNPs were further washed 3 times (12000 rpm, 5 min each time) in deionized water before surface functionalization. To prepare MNP@PA/BSA, the isolated MNPs were added into 1 mg/mL Protein A and BSA mixture (77673, Thermo Fisher Scientific and A7030, Sigma-Aldrich, 1:1 in mass ratio) in Na_2HPO_4/NaH_2PO_4 buffer at pH 8.5 and shaken for 7 h and then washed using deionized H_2O (12000 rpm, 5 min, 3 washes). To prepare MNP@PA/BSA@NcadAb, the MNP@PA/BSA was dispersed in N-cadherin antibody (13116S, Cell Signaling Technology, 100 μg/mL in PBS at pH 7.2) for 1 h at RT and then washed by PBS (12000 rpm, 5 min, 3 washes). The protocol to prepare MNP@BSA was similar to that of MNP@PA/BSA except for the use of 2 mg/mL BSA solution during the surface coating.

Characterization of MNPs. The morphology of bare MNPs and N-cadherin antibody functionalized MNPs was characterized by a JEOL JEM 2100 LaB_6 of 200 kV. Zeta potential and hydrodynamic size of MNPs were analyzed through a Zetasizer Nano ZS system from Malvern Instruments. SEM/EDX (Helios 5 CX DualBeam) was conducted to compare the chemical composition (e.g., the presence of sulfur) of MNPs before and after antibody functionalization. The absorbance spectra of MNPs in different media were collected by a Shimadzu-1900 spectrophotometer.

Cell Culture. HUVEC (PCS-100-010), MDA-MB-231 (HTB-26), PC3-3M (CRL-3471), THP-1 (TIB-202), HL-60 (CCL-240), HCAEC (PCS-100-020), vascular cell basal medium (PCS-100-030), endothelial cell growth kit-VEGF (PCS-100-041), DMEM: F-12 medium (30-2006), RPMI-1640 medium (30-2001), trypsin-EDTA (PCS-999-003), and trypsin neutralizing solution (PCS-999-004) were purchased from ATCC. HDMVEC (CC-2505), EBM-2 basal medium (CC-3156), and an EGM-2 supplement kit (CC-4147) were purchased from LONZA. HUVEC and HCAEC cells were cultured using vascular cell basal medium supplemented with the endothelial cell growth kit-VEGF. HDMVEC cells were cultured using EBM-2 basal medium containing the EGM-2 supplement kit. MDA-MB-231 cells were cultured by using DMEM with 10% FBS. PC3-M cells were cultured by using RPMI-1640 with 10% FBS. THP-1 cells were cultured using RPMI-1640 with 10% FBS and 0.05 mM 2-mercaptoethanol. HL-60 cells were cultured using RPMI-1640 with 10% FBS. Before adhesion and transmigration assays were performed, HL-60 cells were differentiated to neutrophil-like cells by incubating cells in RPMI-1640 containing 1.3% DMSO for 96 h.

Cytotoxicity Assays. The cytotoxicity of MNP@NcadAb was measured by the XTT and LDH assays. In brief, HUVEC and HDMVEC were seeded in 96-well plate (5000 cells per well) and grown for 24 h in 100 μL of growth medium. The medium was then changed to 100 μL of fresh medium with MNP@NcadAb (0, 10, 20, 50, 100, 200, and 400 μg/mL) to culture cells for another 12 h. Each concentration group was performed in five wells/replicates. Next, the XTT and LDH assays were performed following the instructions of the XTT kit (X12223, Thermo Fisher Scientific) and LDH kit (C20301, Thermo Fisher Scientific). Both assays were read out using a BioTek Epoch 2 microplate reader.

Immunostaining of N-Cadherin. Normal HUVEC and HDMVEC cells (as untreated groups) were seeded into a 50 mm glass bottom cell culture dish (5000 cells/cm^2) and cultured for 24 h. For IL-1β treated HUVEC and TGF-β treated HDMVEC, HUVEC and HDMVEC cells were first cultured in a glass-bottom dish for 12 h from the seeding density of 5000 cells/cm^2. Then IL-1β (5 ng/mL, 201-LB, R&D System) or TGF-β (10 ng/mL, PHG9204, Thermo Fisher Scientific) was mixed into the medium, and the cells were cultured for another 12 h. Then the cells were fixed with 4% paraformaldehyde (PFA) (28908, Thermo Fisher Scientific) for 5 min and blocked with BlockAid blocking solution (B10710, Thermo Fisher Scientific) for 30 min at 37 °C. Next, the cells were incubated with N-cadherin antibody (13116S, Cell Signaling Technology,

https://doi.org/10.1021/acsnano.3c12281
ACS Nano 2024, 18, 8229−8247

Rabbit IgG, 1:1000 dilution in BlockAid solution) at 4 °C overnight and then washed by Dulbecco's phosphate-buffered saline (DPBS) (3 washes). Subsequently, anti-rabbit IgG Alexa Flour 488 (4412S, Cell Signaling Technology) was diluted in BlockAid solution (1:500), added into the cells, incubated for 30 min, and washed with DPBS (3 washes). Finally, the cell nucleus was stained with 4′,6-diamidino-2-phenylindole (DAPI). An Olympus IX71 inverted fluorescence microscope with a 100× objective was applied for fluorescence imaging. The quantitative analysis of cell surface N-cadherin was conducted by quantifying the cell area and cell integrated fluorescence intensity using ImageJ. Ten individual cells were analyzed in each treatment group.

Cellular Uptake and Intracellular Localization of MNPs. For tracking the cellular uptake of MNPs, MNP@NcadAb and MNP@BSA were labeled with a similar amount of FITC-BSA (A9771, Sigma-Aldrich). To label MNP@NcadAb, the surface functionalization protocol was adjusted slightly, during which the Protein A and BSA mixed solution used for the unlabeled version of MNP@NcadAb was replaced by a Protein A and FITC-BSA mixed solution (1:1 mass ratio). To label MNP@BSA, BSA solution was substituted by a BSA and FITC-BSA mixed solution (1:1 mass ratio). Normal HUVEC and HDMVEC cells were seeded into a 50 mm glass bottom dish (5000 cells/cm^2) and cultured for 24 h. Afterward, the medium was replaced by new medium with 100 μg/mL FITC-BSA labeled MNP@NcadAb. After 12 h, the cells were washed 3 times with DPBS and fixed by 4% PFA for 5 min. For the cytokine treated endothelial cells, the HUVEC and HDMVEC cells were first cultured for 12 h. Then the medium of HUVEC and HDMVEC cells was changed to fresh medium containing IL-1β (5 ng/mL) or TGF-β (10 ng/mL) to culture cells for another 12 h. After IL-1β and TGF-β treatment, HUVEC and HDMVEC were treated with fresh medium containing FITC-BSA labeled MNP@BSA (100 μg/mL) or FITC-BSA labeled MNP@NcadAb (100 μg/mL) for 12 h. For the free N-cadherin antibody + MNP@NcadAb groups (i.e., the blocking/competition assay), the cytokine activated endothelial cells were first treated with fresh medium containing N-cadherin antibody (10 ug/mL) for 30 min and then cultured with 100 μg/mL FITC-BSA labeled MNPS@NcadAb for 12 h. After 12 h of cell−nanoparticle co-incubation, the medium containing MNPs was discarded, and cells were washed and subjected to fixation for fluorescence imaging. Cell integrated fluorescence intensity in ImageJ was used to quantify the cellular uptake of MNPs. In each group, ten individual cells were analyzed. To investigate the intracellular localization of MNP@NcadAb, the cells were stained with LysoTracker (L7528, Thermo Fisher Scientific). An Olympus IX71 inverted fluorescence microscope with a 100× objective was applied for fluorescence imaging.

Fluorescence Imaging of VE-Cadherin and F-Actin. For the untreated HUVEC and HDMVEC, cells were cultured for 60−80 h to form an endothelial monolayer from the seeding density of 5000 cells/cm^2 in a 50 mm glass bottom dish. For the cytokine activated groups, the HUVEC and HDMVEC monolayers were treated for 12 h with IL-1β (5 ng/mL) and TGF-β (10 ng/mL), respectively. For the MNP@NcadAb treated groups, IL-1β and TGF-β treated monolayers were incubated with MNP@NcadAb (100 μg/mL) for another 12 h before fixation and fluorescence staining. For the fluorescence staining, the monolayer was fixed with 4% PFA for 5 min and permeabilized with 0.1% Triton X-100 for another 5 min, followed by washing with DPBS (3 washes). Next, the monolayer was blocked by BlockAid blocking solution for 30 min at 37 °C and then incubated with VE-cadherin antibody (2500S, Cell Signaling Technology, Rabbit IgG, 1:200 dilution in BlockAid solution) at 4 °C overnight and incubated with anti-rabbit IgG Alexa Flour 488 (1:500 dilution in BlockAid solution) for another 1 h. The F-actin was labeled with ActinRed (R37112, Thermo Fisher Scientific). The cell nuclei were stained by DAPI. An Olympus IX71 inverted fluorescence microscope with a 100× objective was applied for fluorescence imaging.

Endothelial Permeability Assay. HUVEC and HDMVEC (10000−20000 cells in 100 μL of growth medium) were seeded and cultured to 100% confluence monolayers on transwell inserts (3470, Corning). Meanwhile, 600 μL of growth medium was added to the bottom chamber. For cytokine activation, the monolayers were treated with 100 μL of fresh medium containing 5 ng/mL IL-1β (HUVEC) or 10 ng/mL TGF-β (HDMVEC) for 12 h. The old medium in the bottom chamber was changed to 600 μL of fresh medium. For the MNP@NcadAb treated groups, the IL-1β and TGF-β treated monolayers were further treated with MNP@NcadAb (100 μg/mL) for 12 h (100 μL of nanoparticle-containing medium in the top chamber and 600 μL of fresh medium in the bottom chamber). To measure the permeability of endothelial monolayers, the medium in the top chamber was changed to 100 μL of new medium containing FITC-dextran (1 mg/mL, FD-4, Sigma-Aldrich). The bottom chamber medium was changed to 600 μL of new medium. After 30 min of co-incubation with the monolayers, the medium in the bottom chamber was collected and analyzed by a microplate reader (Ex: 490 nm, Em: 520 nm) to measure the FITC-dextran amount that transported across the endothelial monolayers. Each group was performed in five independent inserts.

AFM Imaging of Single Live Cells. Single HUVEC and HDMVEC cells were imaged by a BioScope Resolve AFM (Bruker) using a nanomechanical imaging mode. For the untreated HUVEC and HDMVEC cells, 20000−30000 cells were seeded and cultured overnight in a 50 mm cell culture dish. On the second day, the old medium was replaced with fresh growth medium prior to AFM imaging. For the IL-1β activated HUVEC and TGF-β activated HDMVEC cells, the cells were activated in their monolayer states: HUVEC and HDMVEC monolayers were first prepared in a 50 mm dish and treated with 5 ng/mL IL-1β (HUVEC) and 10 ng/mL TGF-β (HDMVEC) for 12 h. For AFM imaging, the activated HUVEC and HDMVEC cells were trypsinized, seeded, and cultured by using the same protocol as with untreated cells. For the MNP@NcadAb treated groups, after the endothelial monolayers were treated by IL-1β or TGF-β for 12 h, the medium was changed to fresh medium containing 100 μg/mL MNP@NcadAb to culture cells for another 12 h. Then the endothelial cells were trypsinized, seeded, and cultured using the same protocol as with untreated cells for AFM imaging. The detailed AFM imaging protocol was published earlier by our group with minor modifications.[50,51] PFQNM-LC-A-CAL cantilevers (spring constant: ∼0.08 N/m, radius of tip: ∼70 nm) and a 37 °C heating stage were used for endothelial cell imaging. During the live cell imaging, a set of parameters were optimized as follows: 300−500 nm oscillation amplitude, 500−700 pN peak force set point, 0.25 kHz peak force frequency, 0.12 Hz scanning frequency, and 256 × 256 pixels imaging resolution. NanoScope Analysis software was applied to analyze the AFM images and the average Young's modulus of individual cells. The Hertz model was used to fit indentation curves and to calculate Young's modulus. An area of 10 × 10 μm^2 in the central region of cells was selected to analyze the average modulus. The selected central region of cells was thicker than 2 μm, so the substrate effect can be eliminated as the cells were indented for ∼200 nm in depth (1/10 of the cell height). The cell aspect ratio was generated from five individual cells using the cell length divided by the cell width at the midpoint of the cell length.

dSTORM Imaging of Endothelial Cells. The cell sample preparation in different treatment groups for dSTORM imaging remained the same as that for AFM imaging. The detailed dSTORM imaging protocol was published earlier by our group.[50,51] In brief, prior to dSTORM imaging, the cells were fixed with PFA for 5 min, permeabilized with Triton X-100 in cytoskeleton buffer (detailed in Table S1) for 10 min, blocked with 1% BSA for 30 min at RT, incubated with Alexa Fluor 568 Phalloidin (1:400 dilution in PBS, A12380 from Thermo Fisher Scientific) at 4 °C overnight, and finally incubated with the imaging buffer (detailed in Table S2) during the image collection process. An Olympus fluorescence microscope (IX71) and a 100× TIRF objective were used to collect dSTORM images, and data were processed and analyzed through ThunderSTORM in ImageJ. A total of five cells were used to analyze actin orientation.

Adhesion Assay. HUVEC and HDMVEC cells were seeded in a 50 mm cell culture dish (5000 cells/cm^2) and cultured until 100% confluence monolayers were formed. For the cytokine activation, the

https://doi.org/10.1021/acsnano.3c12281
ACS Nano 2024, 18, 8229−8247

monolayers were treated with 5 ng/mL IL-1β (HUVEC) and 10 ng/mL TGF-β (HDMVEC) for 12 h. For the MNP@NcadAb treated groups, the cytokine activated endothelial monolayers were further treated with MNP@NcadAb (100 μg/mL) for another 12 h. To conduct adhesion assays on HUVEC monolayers, 500,000−700,000 Cell Tracker Green (C7025, Thermo Fisher Scientific) labeled HL-60 or THP-1 cells were dropped onto HUVEC monolayers. To conduct adhesion assays on HDMVEC monolayers, 800,000−1,000,000 Cell Tracker Green labeled MDA-MB-231 or PC3-M cells were dropped onto HDMVEC monolayers. After 1 h of waiting for cell attachment, the medium was removed, and the dishes were washed with DPBS (3 washes) to remove unattached cells and further fixed with 4% PFA for 5 min. An Olympus fluorescence microscope (IX71) and a 20× objective were utilized to collect bright field and fluorescence images. For each group, eight random areas from four different dishes were imaged to count adhered cells.

Trans-Endothelial Migration (TEM) Assay. The transwell insert was first coated with fibronectin (120 μg/mL, 33016015, Thermo Fisher Scientific) for 1 h at RT, and then HUVEC and HDMVEC cells were seeded in each insert (10000−20000 cells/insert) and cultured overnight to reach 100% confluence. Then the HUVEC and HDMVEC monolayers were treated with cytokines alone and cytokines followed by MNP@NcadAb as described earlier. To conduct a TEM assay of HL-60 across HUVEC, Cell Tracker Green labeled HL-60 cells were seeded onto the top chamber of the insert. After 1 h of cell attachment, the unattached HL-60 cells were washed, and the old medium was replaced by 100 μL of fresh vascular basal medium, and the bottom chamber medium was changed to 600 μL of endothelial growth medium supplemented with 0.1 μM chemoattractant MLP (F3506, Sigma-Aldrich). After 12 h, the insert (both top and bottom) was fixed with 4% PFA and the cells on the top chamber were scratched off using a cotton swab. Then the bottom surface of the insert was imaged using an Olympus fluorescence microscope (IX71) with a 20× objective. To conduct TEM assays of THP-1, MDA-MB-231, and PC3-M cells, a similar protocol was adopted except for the use of 10% FBS as the chemoattractant in the bottom chamber of the insert. For each group, eight random areas from four different inserts were imaged to count transmigrated cells.

Western Blot. Endothelial and mesenchymal protein markers, total p120, total RhoA, and transcription factors (Snail and Slug) were extracted by RIPA Buffer (89900, Thermo Fisher Scientific). Activated RhoA-GTP was isolated and detected by an Active Rho Kit (16116, Thermo Fisher Scientific). p120 and pp120 (tyrosine phosphorylated p120) were isolated using the N-cadherin antibody and a co-immunoprecipitation kit (26149, Thermo Fisher Scientific). For Western blots, proteins were separated on SDS-PAGE gels at 150 V for 60 min in 1× Tris/Glycine/SDS running buffer (1610772, BioRad), and transferred to a nitrocellulose membrane using a Trans-Blot Turbo Transfer System (1704150, BioRad). Then the membrane was blocked with EveryBlot blocking buffer (12010020, BioRad), incubated with primary antibody (dilution as recommended) overnight at 4 °C, incubated with secondary antibody for 1 h at RT, and finally imaged with a ChemiDoc Imaging System (BioRad). All antibodies and relevant source information are listed in Table S3.

Statistical Analysis. Each experiment was conducted ≥3 times independently or using ≥3 replicates. Quantitative results are presented as mean ± SD. Statistical analysis was performed using GraphPad Prism (V9). Statistical significance among multiple groups was determined by one-way ANOVA with Tukey's post hoc test. The p-values are described in figures and captions as $^{*}p < 0.05$, $^{**}p < 0.01$, $^{***}p < 0.001$, $^{****}p < 0.0001$.

ASSOCIATED CONTENT

Supporting Information

The Supporting Information is available free of charge at https://pubs.acs.org/doi/10.1021/acsnano.3c12281.

SEM-EDX spectra of MNPs; Immunofluorescence staining of N-cadherin; Cellular uptake of MNPs; Co-fluorescence staining of VE-cadherin and F-actin on endothelial monolayers; Endothelial permeability assays of concentration dependency; Monolayer morphology and permeability assays in multiple control groups; AFM and dSTORM images of single cells; Adhesion and TEM assays and data analysis; Migration assays of endothelial cells; Effect of MNPs on IL-1β activated HCAEC and cancer medium activated HUVEC; Uncropped Western blot images and calculation of antibody equivalency; Buffer recipes for dSTORM imaging and antibody source information (PDF)

AUTHOR INFORMATION

Corresponding Author

Congzhou Wang − *Nanoscience and Biomedical Engineering, South Dakota School of Mines and Technology, Rapid City, South Dakota 57701, United States; BioSystems Networks & Translational Research (BioSNTR), Rapid City, South Dakota 57701, United States;* orcid.org/0000-0001-6132-447X; Email: congzhou.wang@sdsmt.edu

Authors

Jinyuan Liu − *Nanoscience and Biomedical Engineering, South Dakota School of Mines and Technology, Rapid City, South Dakota 57701, United States; BioSystems Networks & Translational Research (BioSNTR), Rapid City, South Dakota 57701, United States*

Xiao Yu − *Nanoscience and Biomedical Engineering, South Dakota School of Mines and Technology, Rapid City, South Dakota 57701, United States; BioSystems Networks & Translational Research (BioSNTR), Rapid City, South Dakota 57701, United States*

Annaliese Braucht − *Nanoscience and Biomedical Engineering, South Dakota School of Mines and Technology, Rapid City, South Dakota 57701, United States; BioSystems Networks & Translational Research (BioSNTR), Rapid City, South Dakota 57701, United States*

Steve Smith − *Nanoscience and Biomedical Engineering, South Dakota School of Mines and Technology, Rapid City, South Dakota 57701, United States; BioSystems Networks & Translational Research (BioSNTR), Rapid City, South Dakota 57701, United States*

Complete contact information is available at: https://pubs.acs.org/10.1021/acsnano.3c12281

Notes

The authors declare no competing financial interest.

ACKNOWLEDGMENTS

This work is supported by the National Science Foundation CAREER Award (2143972) and the National Institutes of Health AREA Award (R15CA274349). We thank Reviewer #2 for suggesting control experiments related to nanoparticle endocytosis.

REFERENCES

(1) Bischoff, J. Endothelial-to-Mesenchymal Transition. *Circ. Res.* **2019**, *124*, 1163−1165.

(2) Kovacic, J. C.; Dimmeler, S.; Harvey, R. P.; Finkel, T.; Aikawa, E.; Krenning, G.; Baker, A. H. Endothelial to Mesenchymal Transition in Cardiovascular Disease: JACC State-of-the-Art Review. *J. Am. Coll Cardiol* **2019**, *73*, 190−209.

(3) Piera-Velazquez, S.; Jimenez, S. A. Endothelial to Mesenchymal Transition: Role in Physiology and in the Pathogenesis of Human Diseases. *Physiol. Rev.* **2019**, *99*, 1281−1324.
(4) Sánchez-Duffhues, G.; García de Vinuesa, A.; ten Dijke, P. Endothelial-to-Mesenchymal Transition in Cardiovascular Diseases: Developmental Signaling Pathways Gone Awry. *Dev. Dyn.* **2018**, *247*, 492−508.
(5) Huang, Q.; Gan, Y.; Yu, Z.; Wu, H.; Zhong, Z. Endothelial to Mesenchymal Transition: An Insight in Atherosclerosis. *Frontiers in Cardiovascular Medicine* **2021**, *8*, No. 734550.
(6) Clere, N.; Renault, S.; Corre, I. Endothelial-to-Mesenchymal Transition in Cancer. *Front Cell Dev Biol.* **2020**, *8*, 747.
(7) Li, Y.; Lui, K. O.; Zhou, B. Reassessing Endothelial-to-Mesenchymal Transition in Cardiovascular Diseases. *Nature Reviews Cardiology* **2018**, *15*, 445−456.
(8) Chen, P. Y.; Qin, L.; Baeyens, N.; Li, G.; Afolabi, T.; Budatha, M.; Tellides, G.; Schwartz, M. A.; Simons, M. Endothelial-to-Mesenchymal Transition Drives Atherosclerosis Progression. *J. Clin Invest* **2015**, *125*, 4514−4528.
(9) Alvandi, Z.; Bischoff, J. Endothelial-Mesenchymal Transition in Cardiovascular Disease. *Arterioscler., Thromb., Vasc. Biol.* **2021**, *41*, 2357−2369.
(10) Souilhol, C.; Harmsen, M. C.; Evans, P. C.; Krenning, G. Endothelial-Mesenchymal Transition in Atherosclerosis. *Cardiovasc. Res.* **2018**, *114*, 565−577.
(11) Li, J.; Wang, K.; Pan, W.; Li, N.; Tang, B. Targeted Imaging in Atherosclerosis. *Anal. Chem.* **2022**, *94*, 12263−12273.
(12) Evrard, S. M.; Lecce, L.; Michelis, K. C.; Nomura-Kitabayashi, A.; Pandey, G.; Purushothaman, K. R.; d'Escamard, V.; Li, J. R.; Hadri, L.; Fujitani, K.; Moreno, P. R.; Benard, L.; Rimmele, P.; Cohain, A.; Mecham, B.; Randolph, G. J.; Nabel, E. G.; Hajjar, R.; Fuster, V.; Boehm, M.; Kovacic, J. C. Endothelial to Mesenchymal Transition Is Common in Atherosclerotic Lesions and Is Associated with Plaque Instability. *Nat. Commun.* **2016**, *7*, No. 11853.
(13) Gasparics, Á.; Rosivall, L.; Krizbai, I. A.; Sebe, A. When the Endothelium Scores an Own Goal: Endothelial Cells Actively Augment Metastatic Extravasation through Endothelial-Mesenchymal Transition. *Am. J. Physiol Heart Circ Physiol* **2016**, *310*, H1055−1063.
(14) Platel, V.; Faure, S.; Corre, I.; Clere, N. Endothelial-to-Mesenchymal Transition (Endomt): Roles in Tumorigenesis, Metastatic Extravasation and Therapy Resistance. *Journal of Oncology* **2019**, *2019*, No. 8361945.
(15) Potenta, S.; Zeisberg, E.; Kalluri, R. The Role of Endothelial-to-Mesenchymal Transition in Cancer Progression. *Br. J. Cancer* **2008**, *99*, 1375−1379.
(16) Xu, F.; Guo, H.; Zustiak, S. P.; Genin, G. M. Targeting the Physical Microenvironment of Tumors for Drug and Immunotherapy. *Adv. Drug Delivery Rev.* **2023**, *196*, No. 114768.
(17) Ma, J.; Sanchez-Duffhues, G.; Goumans, M.-J.; ten Dijke, P. TGF-β-Induced Endothelial to Mesenchymal Transition in Disease and Tissue Engineering. *Frontiers in Cell and Developmental Biology* **2020**, *8*, 260.
(18) Pérez, L.; Muñoz-Durango, N.; Riedel, C. A.; Echeverría, C.; Kalergis, A. M.; Cabello-Verrugio, C.; Simon, F. Endothelial-to-Mesenchymal Transition: Cytokine-Mediated Pathways That Determine Endothelial Fibrosis under Inflammatory Conditions. *Cytokine Growth Factor Rev.* **2017**, *33*, 41−54.
(19) Man, S.; Sanchez Duffhues, G.; ten Dijke, P.; Baker, D. The Therapeutic Potential of Targeting the Endothelial-to-Mesenchymal Transition. *Angiogenesis* **2019**, *22*, 3−13.
(20) Luo, L.; Zhang, B.; Tao, F.; Chen, Z.; Ye, Q.; Zhao, X.; Wu, J. Perfluorotributylamine-Loaded Albumin Nanoparticles Downregulate Platelet-Derived TGFβ to Inhibit Tumor Metastasis. *ACS Nano* **2023**, *17*, 15388−15400.
(21) Yoshimatsu, Y.; Watabe, T. Emerging Roles of Inflammation-Mediated Endothelial−Mesenchymal Transition in Health and Disease. *Inflammation and Regeneration* **2022**, *42*, 9.
(22) Wang, Y.; Li, L.; Zhao, W.; Dou, Y.; An, H.; Tao, H.; Xu, X.; Jia, Y.; Lu, S.; Zhang, J.; Hu, H. Targeted Therapy of Atherosclerosis by a Broad-Spectrum Reactive Oxygen Species Scavenging Nanoparticle with Intrinsic Anti-Inflammatory Activity. *ACS Nano* **2018**, *12*, 8943−8960.
(23) Li, J.; Zhao, N.; Zhang, W.; Li, P.; Yin, X.; Zhang, W.; Wang, H.; Tang, B. Assessing the Progression of Early Atherosclerosis Mice Using a Fluorescence Nanosensor for the Simultaneous Detection and Imaging of Ph and Phosphorylation. *Angew. Chem., Int. Ed.* **2023**, *62*, No. e202215178.
(24) Li, J.; Xu, J.; Zhang, W.; Li, P.; Zhang, W.; Wang, H.; Tang, B. Detection and Imaging of Active Substances in Early Atherosclerotic Lesions Using Fluorescent Probes. *ChemBioChem.* **2023**, *24*, No. e202300105.
(25) Wang, S.; Wang, Y.; Lai, X.; Sun, J.; Hu, M.; Chen, M.; Li, C.; Xu, F.; Fan, C.; Liu, X.; Song, Y.; Chen, G.; Deng, Y. Minimalist Nanocomplex with Dual Regulation of Endothelial Function and Inflammation for Targeted Therapy of Inflammatory Vascular Diseases. *ACS Nano* **2023**, *17*, 2761−2781.
(26) He, H.; Han, Q.; Wang, S.; Long, M.; Zhang, M.; Li, Y.; Zhang, Y.; Gu, N. Design of a Multifunctional Nanozyme for Resolving the Proinflammatory Plaque Microenvironment and Attenuating Atherosclerosis. *ACS Nano* **2023**, *17*, 14555−14571.
(27) Ridker, P. M.; Everett, B. M.; Thuren, T.; MacFadyen, J. G.; Chang, W. H.; Ballantyne, C.; Fonseca, F.; Nicolau, J.; Koenig, W.; Anker, S. D.; Kastelein, J. J. P.; Cornel, J. H.; Pais, P.; Pella, D.; Genest, J.; Cifkova, R.; Lorenzatti, A.; Forster, T.; Kobalava, Z.; Vida-Simiti, L.; Flather, M.; Shimokawa, H.; Ogawa, H.; Dellborg, M.; Rossi, P. R. F.; Troquay, R. P. T.; Libby, P.; Glynn, R. J. Antiinflammatory Therapy with Canakinumab for Atherosclerotic Disease. *New England Journal of Medicine* **2017**, *377*, 1119−1131.
(28) Flores, A. M.; Hosseini-Nassab, N.; Jarr, K.-U.; Ye, J.; Zhu, X.; Wirka, R.; Koh, A. L.; Tsantilas, P.; Wang, Y.; Nanda, V.; Kojima, Y.; Zeng, Y.; Lotfi, M.; Sinclair, R.; Weissman, I. L.; Ingelsson, E.; Smith, B. R.; Leeper, N. J. Pro-Efferocytic Nanoparticles Are Specifically Taken up by Lesional Macrophages and Prevent Atherosclerosis. *Nat. Nanotechnol.* **2020**, *15*, 154−161.
(29) Krizbai, I. A.; Gasparics, Á.; Nagyőszi, P.; Fazakas, C.; Molnár, J.; Wilhelm, I.; Bencs, R.; Rosivall, L.; Sebe, A. Endothelial-Mesenchymal Transition of Brain Endothelial Cells: Possible Role During Metastatic Extravasation. *PLoS One* **2015**, *10*, No. e0119655.
(30) Gaikwad, A. V.; Lu, W.; Dey, S.; Bhattarai, P.; Haug, G.; Larby, J.; Chia, C.; Jaffar, J.; Westall, G.; Singhera, G. K.; Hackett, T.-L.; Eapen, M. S.; Sohal, S. S. Endothelial-to-Mesenchymal Transition: A Precursor to Pulmonary Arterial Remodelling in Patients with Idiopathic Pulmonary Fibrosis. *ERJ. Open Research* **2023**, *9*, 00487-2022.
(31) Deng, R.-H.; Zou, M.-Z.; Zheng, D.; Peng, S.-Y.; Liu, W.; Bai, X.-F.; Chen, H.-S.; Sun, Y.; Zhou, P.-H.; Zhang, X.-Z. Nanoparticles from Cuttlefish Ink Inhibit Tumor Growth by Synergizing Immunotherapy and Photothermal Therapy. *ACS Nano* **2019**, *13*, 8618−8629.
(32) Gholami Derami, H.; Gupta, P.; Weng, K.-C.; Seth, A.; Gupta, R.; Silva, J. R.; Raman, B.; Singamaneni, S. Reversible Photothermal Modulation of Electrical Activity of Excitable Cells Using Polydopamine Nanoparticles. *Adv. Mater.* **2021**, *33*, No. 2008809.
(33) Qiu, J.; Shi, Y.; Xia, Y. Polydopamine Nanobottles with Photothermal Capability for Controlled Release and Related Applications. *Adv. Mater.* **2021**, *33*, No. 2104729.
(34) Liu, J.; Kang, L.; Smith, S.; Wang, C. Transmembrane Muc18 Targeted Polydopamine Nanoparticles and a Mild Photothermal Effect Synergistically Disrupt Actin Cytoskeleton and Migration of Cancer Cells. *Nano Lett.* **2021**, *21*, 9609−9618.
(35) Wang, Z.; Luan, J.; Seth, A.; Liu, L.; You, M.; Gupta, P.; Rathi, P.; Wang, Y.; Cao, S.; Jiang, Q.; Zhang, X.; Gupta, R.; Zhou, Q.; Morrissey, J. J.; Scheller, E. L.; Rudra, J. S.; Singamaneni, S. Microneedle Patch for the Ultrasensitive Quantification of Protein Biomarkers in Interstitial Fluid. *Nature Biomedical Engineering* **2021**, *5*, 64−76.
(36) Luan, J.; Seth, A.; Gupta, R.; Wang, Z.; Rathi, P.; Cao, S.; Gholami Derami, H.; Tang, R.; Xu, B.; Achilefu, S.; Morrissey, J. J.;

https://doi.org/10.1021/acsnano.3c12281
ACS Nano 2024, 18, 8229−8247

Singamaneni, S. Ultrabright Fluorescent Nanoscale Labels for the Femtomolar Detection of Analytes with Standard Bioassays. *Nature Biomedical Engineering* **2020**, *4*, 518−530.
(37) Liu, J.; Smith, S.; Wang, C. Photothermal Attenuation of Cancer Cell Stemness, Chemoresistance, and Migration Using Cd44-Targeted Mos2 Nanosheets. *Nano Lett.* **2023**, *23*, 1989−1999.
(38) Medina-Leyte, D. J.; Domínguez-Pérez, M.; Mercado, I.; Villarreal-Molina, M. T.; Jacobo-Albavera, L. Use of Human Umbilical Vein Endothelial Cells (HUVEC) as a Model to Study Cardiovascular Disease: A Review. *Applied Sciences* **2020**, *10*, 938.
(39) Peng, F.; Setyawati, M. I.; Tee, J. K.; Ding, X.; Wang, J.; Nga, M. E.; Ho, H. K.; Leong, D. T. Nanoparticles Promote in Vivo Breast Cancer Cell Intravasation and Extravasation by Inducing Endothelial Leakiness. *Nat. Nanotechnol.* **2019**, *14*, 279−286.
(40) Piera-Velazquez, S.; Jimenez, S. A. Endothelial to Mesenchymal Transition: Role in Physiology and in the Pathogenesis of Human Diseases. *Physiol Rev.* **2019**, *99*, 1281−1324.
(41) Drake, J. M.; Strohbehn, G.; Bair, T. B.; Moreland, J. G.; Henry, M. D. Zeb1 Enhances Transendothelial Migration and Represses the Epithelial Phenotype of Prostate Cancer Cells. *Mol. Biol. Cell* **2009**, *20*, 2207−17.
(42) Voura, E. B.; Sandig, M.; Siu, C.-H. Cell−Cell Interactions During Transendothelial Migration of Tumor Cells. *Microscopy Research and Technique* **1998**, *43*, 265−275.
(43) Oldenburg, J.; de Rooij, J. Mechanical Control of the Endothelial Barrier. *Cell Tissue Res.* **2014**, *355*, 545−555.
(44) Wu, J.; Zhu, Z.; Liu, W.; Zhang, Y.; Kang, Y.; Liu, J.; Hu, C.; Wang, R.; Zhang, M.; Chen, L.; Shao, L. How Nanoparticles Open the Paracellular Route of Biological Barriers: Mechanisms, Applications, and Prospects. *ACS Nano* **2022**, *16*, 15627−15652.
(45) van Buul, J. D.; Timmerman, I. Small Rho Gtpase-Mediated Actin Dynamics at Endothelial Adherens Junctions. *Small GTPases* **2016**, *7*, 21−31.
(46) Lu, L.; Feng, Y.; Hucker, W. J.; Oswald, S. J.; Longmore, G. D.; Yin, F. C. Actin Stress Fiber Pre-Extension in Human Aortic Endothelial Cells. *Cell Motil Cytoskeleton* **2008**, *65*, 281−294.
(47) Escribano, J.; Chen, M. B.; Moeendarbary, E.; Cao, X.; Shenoy, V.; Garcia-Aznar, J. M.; Kamm, R. D.; Spill, F. Balance of Mechanical Forces Drives Endothelial Gap Formation and May Facilitate Cancer and Immune-Cell Extravasation. *PLOS Computational Biology* **2019**, *15*, No. e1006395.
(48) Sisler, J. D.; Pirela, S. V.; Friend, S.; Farcas, M.; Schwegler-Berry, D.; Shvedova, A.; Castranova, V.; Demokritou, P.; Qian, Y. Small Airway Epithelial Cells Exposure to Printer-Emitted Engineered Nanoparticles Induces Cellular Effects on Human Microvascular Endothelial Cells in an Alveolar-Capillary Co-Culture Model. *Nanotoxicology* **2015**, *9*, 769−779.
(49) Wang, M.; Cheng, B.; Yang, Y.; Liu, H.; Huang, G.; Han, L.; Li, F.; Xu, F. Microchannel Stiffness and Confinement Jointly Induce the Mesenchymal-Amoeboid Transition of Cancer Cell Migration. *Nano Lett.* **2019**, *19*, 5949−5958.
(50) Liu, J.; Smith, S.; Wang, C. Reversing the Epithelial−Mesenchymal Transition in Metastatic Cancer Cells Using Cd146-Targeted Black Phosphorus Nanosheets and a Mild Photothermal Treatment. *ACS Nano* **2022**, *16*, 3208−3220.
(51) Kota, D.; Kang, L.; Rickel, A.; Liu, J.; Smith, S.; Hong, Z.; Wang, C. Low Doses of Zeolitic Imidazolate Framework-8 Nanoparticles Alter the Actin Organization and Contractility of Vascular Smooth Muscle Cells. *Journal of Hazardous Materials* **2021**, *414*, No. 125514.
(52) Calzado-Martín, A.; Encinar, M.; Tamayo, J.; Calleja, M.; San Paulo, A. Effect of Actin Organization on the Stiffness of Living Breast Cancer Cells Revealed by Peak-Force Modulation Atomic Force Microscopy. *ACS Nano* **2016**, *10*, 3365−3374.
(53) Dumitru, A. C.; Poncin, M. A.; Conrard, L.; Dufrêne, Y. F.; Tyteca, D.; Alsteens, D. Nanoscale Membrane Architecture of Healthy and Pathological Red Blood Cells. *Nanoscale Horizons* **2018**, *3*, 293−304.
(54) Eghiaian, F.; Rigato, A.; Scheuring, S. Structural, Mechanical, and Dynamical Variability of the Actin Cortex in Living Cells. *Biophys. J.* **2015**, *108*, 1330−1340.
(55) van de Linde, S.; Löschberger, A.; Klein, T.; Heidbreder, M.; Wolter, S.; Heilemann, M.; Sauer, M. Direct Stochastic Optical Reconstruction Microscopy with Standard Fluorescent Probes. *Nat. Protoc.* **2011**, *6*, 991−1009.
(56) Dempsey, G. T.; Vaughan, J. C.; Chen, K. H.; Bates, M.; Zhuang, X. Evaluation of Fluorophores for Optimal Performance in Localization-Based Super-Resolution Imaging. *Nat. Methods* **2011**, *8*, 1027−1036.
(57) Xu, J.; Ma, H.; Liu, Y. Stochastic Optical Reconstruction Microscopy (Storm). *Current Protocols in Cytometry* **2017**, *81*, 12.46.1−12.46.27.
(58) Li, J.; Shi, S.; Srivastava, S. P.; Kitada, M.; Nagai, T.; Nitta, K.; Kohno, M.; Kanasaki, K.; Koya, D. Fgfr1 Is Critical for the Anti-Endothelial Mesenchymal Transition Effect of N-Acetyl-Seryl-Aspartyl-Lysyl-Proline Via Induction of the Map4k4 Pathway. *Cell Death & Disease* **2017**, *8*, e2965−e2965.
(59) Choi, K. J.; Nam, J.-K.; Kim, J.-H.; Choi, S.-H.; Lee, Y.-J. Endothelial-to-Mesenchymal Transition in Anticancer Therapy and Normal Tissue Damage. *Experimental & Molecular Medicine* **2020**, *52*, 781−792.
(60) Gao, Y.; Ouyang, Z.; Shen, S.; Yu, H.; Jia, B.; Wang, H.; Shen, M.; Shi, X. Manganese Dioxide-Entrapping Dendrimers Co-Deliver Protein and Nucleotide for Magnetic Resonance Imaging-Guided Chemodynamic/Starvation/Immune Therapy of Tumors. *ACS Nano* **2023**, *17*, 23889−23902.
(61) Taulet, N.; Comunale, F.; Favard, C.; Charrasse, S.; Bodin, S.; Gauthier-Rouvière, C. N-Cadherin/P120 Catenin Association at Cell-Cell Contacts Occurs in Cholesterol-Rich Membrane Domains and Is Required for Rhoa Activation and Myogenesis. *J. Biol. Chem.* **2009**, *284*, 23137−23145.
(62) Barcelona-Estaje, E.; Dalby, M. J.; Cantini, M.; Salmeron-Sanchez, M. You Talking to Me? Cadherin and Integrin Crosstalk in Biomaterial Design. *Adv. Healthc Mater.* **2021**, *10*, No. e2002048.
(63) Zeng, Q.; Li, W.; Lu, D.; Wu, Z.; Duan, H.; Luo, Y.; Feng, J.; Yang, D.; Fu, L.; Yan, X. Cd146, an Epithelial-Mesenchymal Transition Inducer, Is Associated with Triple-Negative Breast Cancer. *Proc. Natl. Acad. Sci. U. S. A.* **2012**, *109*, 1127−1132.
(64) Kourtidis, A.; Ngok, S. P.; Anastasiadis, P. Z. P120 Catenin: An Essential Regulator of Cadherin Stability, Adhesion-Induced Signaling, and Cancer Progression. *Prog. Mol. Biol. Transl Sci.* **2013**, *116*, 409−32.
(65) Pal, M.; Bhattacharya, S.; Kalyan, G.; Hazra, S. Cadherin Profiling for Therapeutic Interventions in Epithelial Mesenchymal Transition (Emt) and Tumorigenesis. *Exp. Cell Res.* **2018**, *368*, 137−146.
(66) Seidel, B.; Braeg, S.; Adler, G.; Wedlich, D.; Menke, A. E- and N-Cadherin Differ with Respect to Their Associated P120ctn Isoforms and Their Ability to Suppress Invasive Growth in Pancreatic Cancer Cells. *Oncogene* **2004**, *23*, 5532−5542.
(67) Anastasiadis, P. Z.; Moon, S. Y.; Thoreson, M. A.; Mariner, D. J.; Crawford, H. C.; Zheng, Y.; Reynolds, A. B. Inhibition of Rhoa by P120 Catenin. *Nat. Cell Biol.* **2000**, *2*, 637−644.
(68) Huang, N.; Liu, Y.; Fang, Y.; Zheng, S.; Wu, J.; Wang, M.; Zhong, W.; Shi, M.; Xing, M.; Liao, W. Gold Nanoparticles Induce Tumor Vessel Normalization and Impair Metastasis by Inhibiting Endothelial Smad2/3 Signaling. *ACS Nano* **2020**, *14*, 7940−7958.
(69) Piera-Velazquez, S.; Li, Z.; Jimenez, S. A. Role of Endothelial-Mesenchymal Transition (Endomt) in the Pathogenesis of Fibrotic Disorders. *Am. J. Pathol.* **2011**, *179*, 1074−1080.
(70) Lovisa, S.; Fletcher-Sananikone, E.; Sugimoto, H.; Hensel, J.; Lahiri, S.; Hertig, A.; Taduri, G.; Lawson, E.; Dewar, R.; Revuelta, I.; Kato, N.; Wu, C.-J.; Bassett, R. L.; Putluri, N.; Zeisberg, M.; Zeisberg, E. M.; LeBleu, V. S.; Kalluri, R. Endothelial-to-Mesenchymal Transition Compromises Vascular Integrity to Induce Myc-Mediated Metabolic Reprogramming in Kidney Fibrosis. *Science Signaling* **2020**, *13*, No. eaaz2597.

https://doi.org/10.1021/acsnano.3c12281
ACS Nano 2024, 18, 8229−8247

(71) Sun, X.; Nkennor, B.; Mastikhina, O.; Soon, K.; Nunes, S. S. Endothelium-Mediated Contributions to Fibrosis. *Seminars in Cell & Developmental Biology* **2020**, *101*, 78−86.
(72) Jia, Y.; Hu, J.; An, K.; Zhao, Q.; Dang, Y.; Liu, H.; Wei, Z.; Geng, S.; Xu, F. Hydrogel Dressing Integrating Fak Inhibition and Ros Scavenging for Mechano-Chemical Treatment of Atopic Dermatitis. *Nat. Commun.* **2023**, *14*, 2478.
(73) Setyawati, M. I.; Tay, C. Y.; Chia, S. L.; Goh, S. L.; Fang, W.; Neo, M. J.; Chong, H. C.; Tan, S. M.; Loo, S. C. J.; Ng, K. W.; Xie, J. P.; Ong, C. N.; Tan, N. S.; Leong, D. T. Titanium Dioxide Nanomaterials Cause Endothelial Cell Leakiness by Disrupting the Homophilic Interaction of Ve−Cadherin. *Nat. Commun.* **2013**, *4*, 1673.
(74) Setyawati, M. I.; Wang, Q.; Ni, N.; Tee, J. K.; Ariga, K.; Ke, P. C.; Ho, H. K.; Wang, Y.; Leong, D. T. Engineering Tumoral Vascular Leakiness with Gold Nanoparticles. *Nat. Commun.* **2023**, *14*, 4269.
(75) Yamawaki, H.; Iwai, N. Mechanisms Underlying Nano-Sized Air-Pollution-Mediated Progression of Atherosclerosis: Carbon Black Causes Cytotoxic Injury/Inflammation and Inhibits Cell Growth in Vascular Endothelial Cells. *Circ J.* **2006**, *70*, 129−140.
(76) Shi, J.; Sun, X.; Lin, Y.; Zou, X.; Li, Z.; Liao, Y.; Du, M.; Zhang, H. Endothelial Cell Injury and Dysfunction Induced by Silver Nanoparticles through Oxidative Stress Via Ikk/Nf-Kb Pathways. *Biomaterials* **2014**, *35*, 6657−6666.
(77) Setyawati, M. I.; Tay, C. Y.; Bay, B. H.; Leong, D. T. Gold Nanoparticles Induced Endothelial Leakiness Depends on Particle Size and Endothelial Cell Origin. *ACS Nano* **2017**, *11*, 5020−5030.
(78) Xu, Y.; Guo, Y.; Zhang, C.; Zhan, M.; Jia, L.; Song, S.; Jiang, C.; Shen, M.; Shi, X. Fibronectin-Coated Metal−Phenolic Networks for Cooperative Tumor Chemo-/Chemodynamic/Immune Therapy Via Enhanced Ferroptosis-Mediated Immunogenic Cell Death. *ACS Nano* **2022**, *16*, 984−996.
(79) Sun, T.; Zhang, Y. S.; Pang, B.; Hyun, D. C.; Yang, M.; Xia, Y. Engineered Nanoparticles for Drug Delivery in Cancer Therapy. *Angew. Chem., Int. Ed.* **2014**, *53*, 12320−12364.
(80) Wang, Y.; Li, W.; Li, Z.; Mo, F.; Chen, Y.; Iida, M.; Wheeler, D. L.; Hu, Q. Active Recruitment of Anti-Pd-1-Conjugated Platelets through Tumor-Selective Thrombosis for Enhanced Anticancer Immunotherapy. *Science Advances* **2023**, *9*, No. eadf6854.

https://doi.org/10.1021/acsnano.3c12281
ACS Nano 2024, 18, 8229−8247